A Novel Solar Photovoltaic Array Reconfiguration Technique Using Two-Dimensional Generalized Arnold's Cat Map

Rayappa David Amar Raj
Department of Electrical Engineering,
National Institute of Technology,
Warangal, Telangana 506004, India
e-mail: rd721025@student.nitw.ac.in

Kanasottu Anil Naik
Department of Electrical Engineering,
National Institute of Technology,
Warangal, Telangana 506004, India
e-mail: anilnaik205@nitw.ac.in

This paper presents a highly efficient image encryption-based Arnold's cat map (ACM) technique to reconfigure the photovoltaic (PV) array to enhance the output and mitigate the mismatch losses due to partial shading (PS). The proposed ACM technique concentrates on alleviating the power loss by effectively dispersing the shade over the entire PV array without modifying its electrical circuitry. The proposed reconfiguration technique is investigated and analyzed with conventional series–parallel and total-cross-tied configurations along with the recently reported chaotic Baker's map, odd–even, odd–even–prime pattern-based configurations. The proposed technique is examined for symmetrical 6 × 6 PV array and unsymmetrical 6 × 9 PV array under distinct nonuniform and uniform PS cases. To confirm the potency and superior performance of the proposed technique, the system has been extensively examined with nine performance parameters such as global maximum power, mismatch power, power loss, efficiency, fill factor, array yield, capacity factor, performance ratio, and the number of maximum power peaks. An experimental setup of a 4 × 4 array reconfiguration system prototype is developed and tested in a real-time environment to validate the effectiveness of the proposed technique over the existing ones. From the comprehensive investigation, it is regarded that the proposed technique offers consistently superior performance with the least percentage mismatch losses and maximum power enhancement of 48.8%, 31.03%, and 27.5% for various shading cases of 6 × 6 and 6 × 9 PV arrays. [DOI: 10.1115/1.4054506]

Keywords: partial shading, reconfiguration, shade dispersion, power enhancement, Arnold's cat map, efficiency, energy, photovoltaics, renewable, solar, sustainability

1 Introduction

Amongst the available renewable power generation technologies, solar power generation has a leading edge over others in many aspects. However, the solar panels in the solar photovoltaic (PV) system are inevitably shadowed due to various factors [1] and thus lead to a lower output. The power loss is highly dependent on the insolation levels, partial shading (PS) patterns, and shading concentration area. The phenomenon of shading leads to the formation of hotspots which further leads to fire hazards and eventually devastates the module. These hotspots can be avoided by installing bypass diodes across the panels. Nevertheless, installing these diodes results in multiple peaks in the array of PV characteristics [2]. To lessen the effects of shadowing, efficient maximum power point tracking (MPPT) controllers are employed in an array. But these techniques require complex power converters and control algorithms. Despite its better technical performance, employing these controllers makes the system cost-ineffective and infeasible for large-rated PV systems. Due to the above-mentioned limitations of MPPT controllers, reconfiguration techniques act as the best alternative to resolve this issue [3].

The reconfiguration techniques are classified as static and dynamic reconfiguration techniques. The literature review of some notable dynamic reconfiguration techniques includes the employment of enhanced dynamic programming approaches such as smart choice and the Munkres assignment algorithm [4] to attain the irradiance equalization (IE) of rows in a PV array. Nonetheless, the execution of these techniques requires complex programming techniques and complicated circuitry. To optimize the PV array configuration in less computing time and without necessitating working out complex dynamic programming (DP) solutions, the authors in Ref. [5] have proposed a greedy algorithm-based improved reconfiguration scheme. Nevertheless, this method requires three laborious steps for evolving the algorithm. Furthermore, the approach processes numerous reconfiguration solutions till it obtains the best-optimized solution. Despite its effectiveness, the dynamic reconfiguration techniques involve numerous complicated switches and sensors, complex algorithms and controlling units, efficient driver circuits, systematic monitoring units increasing the system complexity and cost. For instance, the number of switches necessitated to dynamically reconfigure a 9 × 9 PV array is 1384 [6].

The static array reconfiguration schemes are regarded as the best alternative to evade the setbacks and challenges of dynamic reconfiguration. In Ref. [7], the authors suggested a static reconfiguration procedure based on sudoku puzzle to dispense the shading in the array. A modified version of the sudoku-based technique named optimal sudoku reconfiguration scheme is reported in Ref. [8] to mitigate the mismatch. Nonetheless, the above two methods cannot modify the elements in the first column of the array which leads to curtailment in output. To amend the shortcomings of the aforementioned two methods, a reconfiguration scheme based on a modified sudoku puzzle exercising a backtracking technique has been proposed in Ref. [9]. In Refs. [10,11], the authors proposed a shadow dispersal approach based on the arrow sudoku (AS) puzzle pattern and tom-tom puzzle pattern, respectively, to enhance the output during dynamic shading. However, both these techniques cannot disperse the first column shade. The authors in Ref. [12] employed an optimized reconfiguration technique to diminish the effects of mutual shading irrespective of the shading

Contributed by the Solar Energy Division of ASME for publication in the Journal of Solar Energy Engineering: Including Wind Energy and Building Energy Conservation. Manuscript received September 2, 2021; final manuscript received April 30, 2022; published online May 31, 2022. Assoc. Editor: Brendan O'Connor.

factors like the sun's position, system's latitude, and the installation aspects. The lower gap between the PV arrays leads to mutual shading (MS) problems. In order to reduce these effects of MS, a static reconfiguration technique that yields the best optimal solution is proposed in Ref. [13].

In [14], the authors proposed a reconfiguration scheme based on Lo-shu magic square for reconfiguring the array under PS. However, this scheme is only confined to a 9×9 array size. Many of the reconfiguration techniques are not employable for both non-symmetrical and symmetrical arrays. A new reconfiguration strategy based on the skyscraper puzzle has been implemented in Ref. [15] for a 6×6 PV array to extract the maximum power and also to reduce the line losses. A polycube puzzle-based dancing-links (DL) algorithm has been employed in Ref. [16] to resolve the sudoku 6×6 grid. For real-time examination, a shifting cloud pattern considering the direction and speed of the wind with distinct instants has been considered. The authors in Ref. [17] developed a magic square (MS) puzzle-based reconfiguration by employing a GA toolbox in MATLAB. The puzzle-based approaches are not compatible with all array sizes and hence they cannot be generalized. Moreover, these approaches disperse the shade in a particular column instead of the entire array [18]. In order to disperse the shade over the PV array for mitigating the mismatch loss, the authors in Ref. [19] implemented a shade distribution process that takes place in two distinct phases for a 9×9 array. However, the results showed that the efficacy of this technique under a short narrow shading pattern is inadequate. In Refs. [20,21], the authors introduced a diagonally distributed TCT reconfiguration technique and a new-column index (NCI) scheme for shade dispersal.

It is noted that the majority of the aforementioned reconfiguration techniques are neither compatible nor applicable to large-rated PV arrays. Besides, all these techniques fail to disperse the shade discriminately. To overcome these limitations, the researchers are looking toward other alternative and unexplored strategies based on the concept of image encryption. Very recently, a novel image processing-based array reconfiguration motivated by the chaotic Baker's map (CBM) has been proposed in Refs. [22,23]. By employing the CBM technique, optimal power output is obtained by mitigating the mismatch in the array row currents. Despite its better performance with respect to conventional PV array configurations, the CBM technique inherits the following shortcomings: (a) ineffective shade dispersal over the entire PV array and (b) inapplicability for all sizes of PV array. Very recently, the odd–even (OE) [24] and odd–even–prime (OEP) [25] pattern-based reconfiguration techniques that are compatible for all array sizes are proposed to mitigate the shading impacts. Despite being applicable for all arrays, they fail to uniformly disperse the shade. Therefore, a highly efficient reconfiguration technique that rectifies the above-mentioned shortcomings is needed and is proposed in the present work.

The major highlights of the proposed work are as follows:

- In contrast to many static reconfiguration techniques [7–17,19–23,26–28], the proposed technique is applicable to various sizes of PV array such as 6×6, 3×5, 7×5, 11×18, etc. and further it disperses the shade discriminately and uniformly over the entire array. Here, the shade dispersion is attained based on an encryption technique where the correlation between the adjacent shaded modules in a row are highly reduced thereby augmenting the total irradiation of the row.
- The potency of the proposed technique is compared with the conventional along with the recently proposed image processing-based CBM [22,23], OE [24], OEP [25] configurations under distinct shading patterns of a 6×6 symmetrical PV array and a 6×9 unsymmetrical PV array.
- A detailed shade dispersion and comparative analysis of row current variation of all configurations under distinct shading cases are presented.

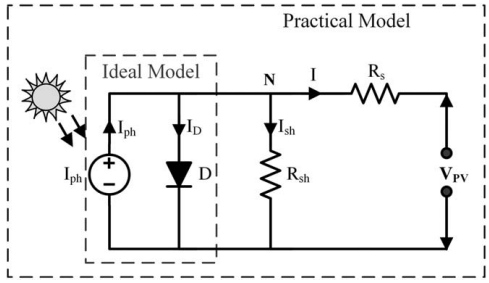

Fig. 1 Equivalent circuit of PV cell

- An experimental setup of a 4×4 array reconfiguration system prototype is developed and tested under real-time environment to validate the effectiveness of proposed configuration over the existing ones.

2 Modeling of Photovoltaic Cell

Numerous modeling approaches that are reported in the literature are single-diode model, double-diode model, and three-diode model [29]. In this research, a single-diode equivalent circuit model is employed for modeling due to its simplicity as shown in Fig. 1.

By employing KCL at the junction "N", the PV cell output current (I) is obtained as follows:

$$I = I_{\mathrm{Ph}} - I_{\mathrm{D}} - \frac{V_{\mathrm{PV}} + IR_{\mathrm{s}}}{R_{\mathrm{sh}}} \tag{1}$$

where "I_{ph}" is the photon current generated, "I_{D}" is the diode current, "R_{s}" is the series resistor, "R_{sh}" is the shunt resistor, "V_{PV}" is the cell output voltage, and "I" is the cell output current. The ideal diode current equation is formulated as

$$I_{\mathrm{D}} = I_0 \times \left[\exp\left(\frac{V_{\mathrm{D}}}{\alpha V_{\mathrm{T}}}\right) - 1\right] \tag{2}$$

where "I_0" is the module reverse saturation current, "α" is the diode ideality factor, and "V_{T}" is the thermal voltage which is given by

$$V_{\mathrm{T}} = \frac{N_{\mathrm{S}} \times k \times T}{q} \tag{3}$$

where "N_{S}" is the number of series-connected cells, "k" is the Boltzmann constant, "T" is the temperature of module, and "q" is the electron charge, 1.60217×10^{-19} C. The array current (I) is determined employing the below equation

$$I = N_{\mathrm{PP}}\left(I_{\mathrm{Ph}} - I_0\left(\exp\left(\frac{V_{\mathrm{PV}} + IR_{\mathrm{s}}}{V_{\mathrm{T}} N_{\mathrm{ss}}}\right) - 1\right)\right) - \left(\frac{V_{\mathrm{PV}} + IR_{\mathrm{s}}}{R_{\mathrm{sh}}}\right) \tag{4}$$

where "N_{pp}" and "N_{ss}" are the number of parallel-connected and series-connected PV modules.

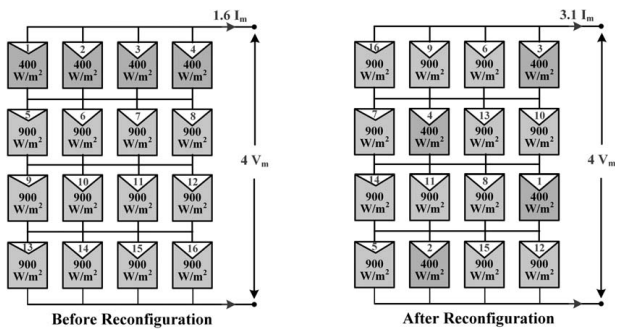

Fig. 2 Irradiation equalization of rows through effective reconfiguration

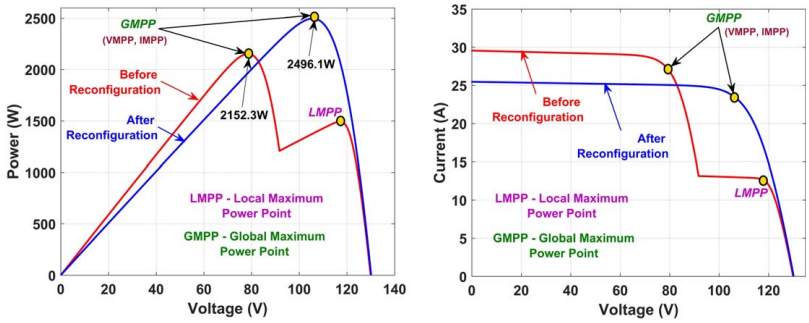

Fig. 3 Power–voltage and current–voltage characteristics of PV array (at $T = 25$ °C)

3 Partial Shading Conditions

The PV array experiences diverse irradiation levels leading to partial shading phenomena that limits the output significantly. The shading can be uniform or nonuniform based on the source of shading. In some cases, the shading due to high-rise buildings, clouds, elevated towers, and poles is uniform in nature as there exist very gentle irradiation transitions causing only minor irradiation differences between the adjacent shaded PV panels. Besides, the array is also subjected to nonuniform shading where there exists a considerable irradiance difference between the adjacent shaded panels. The uneven reception of irradiation can be due to the irregular shadowing of trees, bird droppings, high concentration of dirt and dust particles in a specific area, etc.

3.1 Conventional Photovoltaic Array Configurations. To obtain rated output, the PV panels are connected in various conventional configurations such as series (S), parallel (P), series–parallel (SP), honey-comb (HC), bridge-linked (BL), and total-cross-tied (TCT) PV array configurations. Among all the available conventional configurations, TCT configuration yields more power output during PS [30]. Even though TCT configuration holds a larger potential to achieve maximum output, it suffers from some impediments like zero shade dispersal and the advent of multiple power peaks under PS. So, there is a dire need for reconfiguring the PV array for effective shade dispersal.

3.2 Reconfiguration of Solar Photovoltaic Array. From the comprehensive literature review, it is noted that reconfiguring the array effectively mitigates the impacts of shading. It is performed either by optimally rewiring the electrical connections of the PV array or by relocating the panels without altering the electrical circuitry. The practical feasibility of the static reconfiguration is confirmed extensively [7–25] as it is a one-time optimal interconnection that can be executed during the installation time itself. Besides, unlike the dynamic reconfiguration, it is also an economically feasible strategy as it doesn't necessitate any sensors, switches, relays, switching controllers, etc., to reconfigure the panels. The shade dispersion through effective reconfiguration of array for equalizing the irradiation between rows is shown in Fig. 2. It is observed that TCT configured PV array has the panel numbers 1–4 in the first row, 5–8 in the second row, and so on. For instance, the first row of the PV array is shaded receiving a lower irradiation of 400 W/m^2 whereas the unshaded panels receive a maximum irradiation of 900 W/m^2. Hence, the current generated by the first row is highly reduced thereby increasing the mismatch between the row currents and limiting the total array current to $1.6I_m$. So, the PV array is effectively reconfigured to disperse the shade uniformly over the entire array minimizing the mismatch between rows and hence enhancing the total array current to $3.1I_m$ resulting in improved array characteristics as shown in Fig. 3. Before reconfiguration, the row current mismatch is from $1.6I_m$ to $3.6I_m$ resulting in two MPPs with GMP of 2152.3 W. After reconfiguration, the row current mismatch drops to zero where all the rows generate $3.1I_m$ current, exhibiting only one power peak with the enhanced GMP of 2496.1 W. Mitigating the MPPs through uniform shade dispersion reduces the cost, complexity and computational burden on MPPT controllers to track GMPP effectively.

3.3 Drawbacks of Existing Reconfiguration Approaches. Despite the existence of many static reconfiguration techniques, a majority of them have severe limitations. The best reconfiguration strategy must be compatible with all arrays, and must be rigid enough to disperse the shade uniformly irrespective of shading pattern mitigating the row current variation and local MPPs. The existing approaches fulfill these criteria only to some extent hence yielding a suboptimal output. For instance, the puzzle-based approaches [8–13,15,16,26–28], magic square-based approaches [14,17], existing CBM [22,23] cannot be applicable to unsymmetrical arrays sizes. To overcome this drawback an odd–even [24] and odd–even–prime [25] pattern-based reconfiguration techniques are reported. However, these techniques despite being applicable to all array sizes fail to disperse the shade uniformly due to their poor and ineffective reconfiguration strategies, thus increasing the mismatch and MPPs. Therefore, in this work, a novel Arnold's cat map-based array reconfiguration is proposed.

4 Proposed Methodology

Generally, a digital image is considered to be a matrix comprising of pixels. In image encryption, the security of the image is enhanced by operating it with a transformation, which repositions the original location of its pixels [31]. A popular chaotic map such named Arnold's cat map is one of the regularly employed tools for image encryption process.

4.1 Arnold's Cat Map Technique. A 2D Arnold's cat map (ACM) is a simplistic and sophisticated illustration of some principles of chaotic dynamics—particularly, underlying order to a stochastic development of a system [32]. Arnold determined to demonstrate this technique by employing a crude picture of a cat. Consecutive applicability of ACM transformation stretches and shear the image of a cat, and later wrapped back into a unit square. The stretching and wrapping maintain the volume, however, the image is all jumbled up, quite like blending as chaos in the Hamiltonian system.[1] The mapping retains and combines areas, and is also reversible.

Furthermore, as this transformation is implemented sequentially, it provides a consecutive range of transformed values that become thinner till the unit square is evenly blended as shown in Fig. 4. The basic Arnold's cat map (ACM) is described by the equation

[1]https://galileo-unbound.blog/2019/06/16/vladimir-arnolds-cat-map/

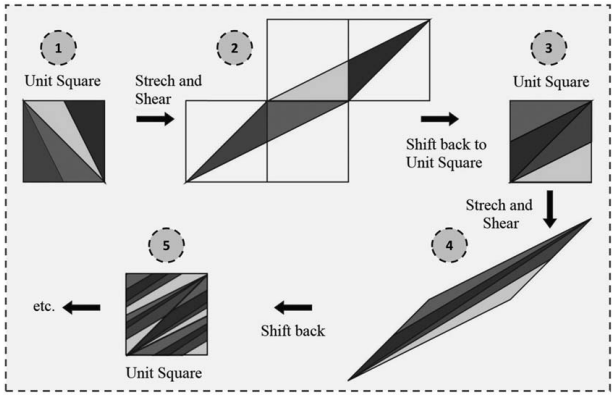

Fig. 4 Geometrical description of ACM technique

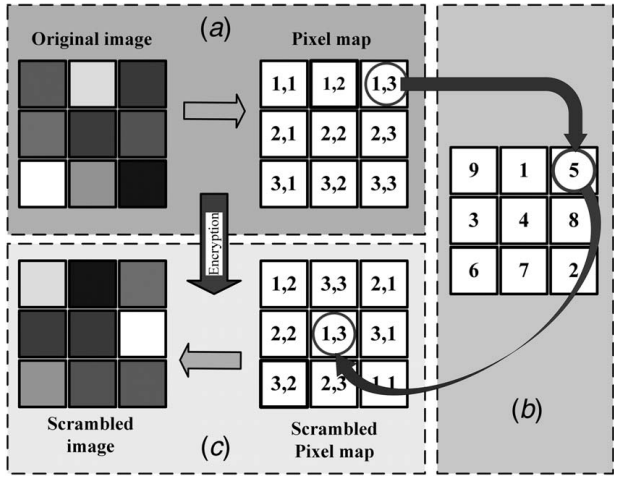

Fig. 5 Image encryption process: (*a*) original image, (*b*) rearranged matrix, and (*c*) scrambled image

as follows [32]:

$$\begin{pmatrix} x(i+1) \\ y(i+1) \end{pmatrix} = \begin{pmatrix} 1 & 1 \\ 1 & 2 \end{pmatrix} * \begin{pmatrix} x(i) \\ y(i) \end{pmatrix} \bmod N \tag{5}$$

where $x(i)$ and $y(i) \in \{0, 1, 2, 3, \ldots..N-1\}$, the ACM is discretized and "mod" is modulus of

$$\begin{pmatrix} x(i)+y(i) \\ x(i)+2\times y(i) \end{pmatrix}$$

and the order of matrix "N" which designates the size of an image. In image encryption, $[x(0), y(0)]^T$ represents the initial pixel coordinates, and by employing ACM, all these pixel coordinates are transformed to new pixel coordinates $[x(i), y(i)]^T$ after "i" iterations and eventually, a permutated image is obtained. A superior encryption strategy can be designed by selecting an elongated period "P". This is ascertained by determining the period "P" of the discrete ACM. The period of discretized ACM does not invariably become longer by an increasing modulo. For the generalized ACM, its period does not invariably expand by increasing the parameters. Hence, it is significant to determine the correlation between the period, modulo, and its parameters. In Ref. [33], the correlation between the minimum period $\Pi(N)$ of discrete ACM and its order "N" is described as follows:

$$\Pi(N) = \begin{cases} 3N & \text{if and only if } N = 2\times 5^k \text{ for } k = 1, 2, 3, \ldots. \text{and so on} \\ 2N & \text{if and only if } N = 5^k \text{ or } N = 6\times 5^k \text{ for } k = 1, 2, 3, \ldots \\ \dfrac{12N}{7} & \text{for all other values of } 'N' \end{cases}$$

Now, the ACM equation given in Eq. (5) is generalized with the incorporation of two control parameters "a" and "b," where "a" and "b" are positive integers, whose values are randomly chosen between the lower and upper bounds of total iterations performed on an image that is to be encrypted [34]. The generalized ACM is given as follows:

$$\begin{pmatrix} x(i+1) \\ y(i+1) \end{pmatrix} = \begin{pmatrix} 1 & a \\ b & ab+1 \end{pmatrix} * \begin{pmatrix} x(i) \\ y(i) \end{pmatrix} \bmod N \tag{6}$$

$$\begin{pmatrix} x(i+1) \\ y(i+1) \end{pmatrix} = A * \begin{pmatrix} x(i) \\ y(i) \end{pmatrix} \bmod N \tag{7}$$

$$\text{where} \quad A = \begin{pmatrix} 1 & a \\ b & ab+1 \end{pmatrix}$$

For a given value of "N", $\Pi(N)$ indicates minimum period. The matrix "A" is now expressed as follows:

$$A^n = \begin{pmatrix} u_{2n-1} & u_{2n} \\ u_{2n} & u_{2n+1} \end{pmatrix}$$

$$\begin{pmatrix} x(i+1) \\ y(i+1) \end{pmatrix} = \begin{pmatrix} u_{2n-1}x(i) + u_{2n}y(i) \\ u_{2n}x(i) + u_{2n+1}y(i) \end{pmatrix} \bmod N \tag{8}$$

where "u_n" is the Fibonacci number and "P" is the period of cat map shown in Eq. (8), given that either of the below conditions are satisfied [33]:

(1) $u_{2P-1} \equiv 1 \pmod N$ and $N | u_{2P}$
(2) $u_{2P} \equiv 0 \pmod N$ and $N | u_{2P}$
(3) $u_{2P+1} \equiv 1 \pmod N$ and $N | u_{2P}$

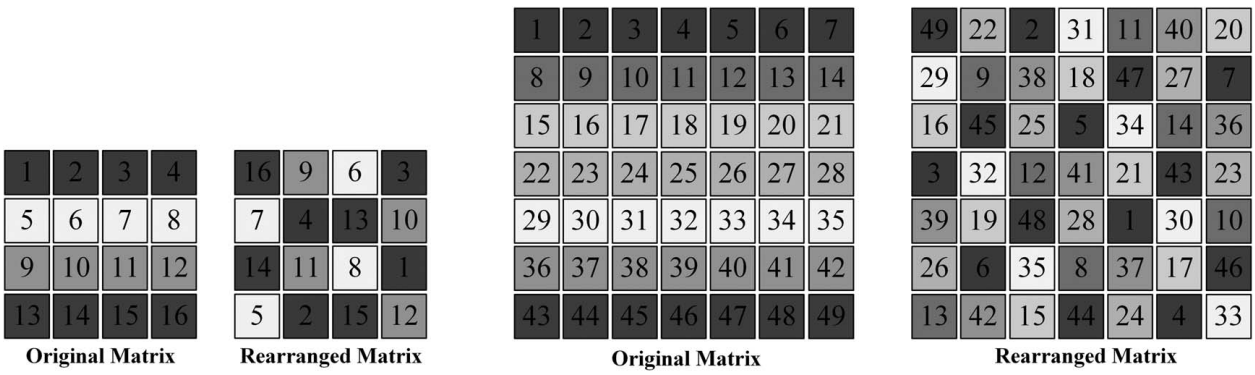

Fig. 6 Original matrix and its corresponding reconfigured matrix obtained by the proposed ACM

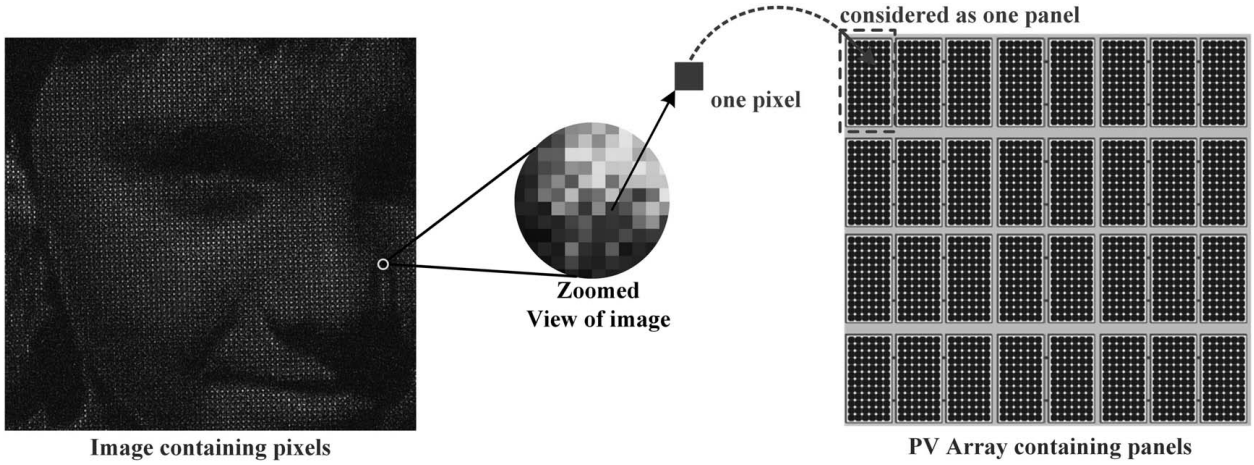

Fig. 7 Image of pixels analogous to solar PV array

Equation (5) has a stable point always as it consists of homogenous linear equations and the stable point of ACM is $\begin{cases} x^* = 0 \\ y^* = 0 \end{cases}$. The Jacobian matrix of ACM is $\begin{bmatrix} 1 & 1 \\ 1 & 2 \end{bmatrix}$ and its eigenvalues are computed as $\lambda_1 = 3 + \sqrt{5}/2 = 2.62$ and $\lambda_2 = 3 - \sqrt{5}/2 = 0.38$. Furthermore, the eigenvalues of the Jacobian matrix of generalized ACM are $\lambda_1 = 1 + ab + \sqrt{(ab+2)^2 - 4}/2 > 1$ and $\lambda_2 = 1 + ab - \sqrt{(ab+2)^2 - 4}/2 < 1$. The ACM is always chaotic for the values (a and b) > 0. Hence, the stable point (0, 0) is a saddle point as it has one positive and negative Lyapunov characteristic exponents. So, ACM is chaotic as it holds one positive Lyapunov characteristic exponent [34].

It is observed from the detailed pictorial description of image encryption shown in Fig. 5 that the original image of 3 × 3 order contains the nine pixels of distinct colors. When this image is applied with ACM, its pixels are scrambled effectively based on the rearranged ACM matrix (Fig. 5(*b*)). For example, the red-colored pixel is originally located in (1,3) coordinates and after applying ACM, it has been moved to new coordinates (second row and second column). Similarly, all the coordinates are effectively rearranged which results in scrambled image as shown in Fig. 5(*c*). Accordingly, the original matrix positions and their corresponding reconfigured matrix obtained by the proposed ACM of a 4 × 4, and 7 × 7 matrices are shown in Fig. 6. Besides, the original and rearranged matrices obtained by existing OE, OEP techniques are shown in Fig. 29 of the Appendix. The flowchart of PV array reconfiguration technique using ACM algorithm is shown in Fig. 9.

4.2 Application of Arnold's Cat Map in Photovoltaic Array Reconfiguration. ACM is the well-known chaotic map approach which rearranges the pixels of an image for better security purposes. This is performed by transferring the pixels from their original

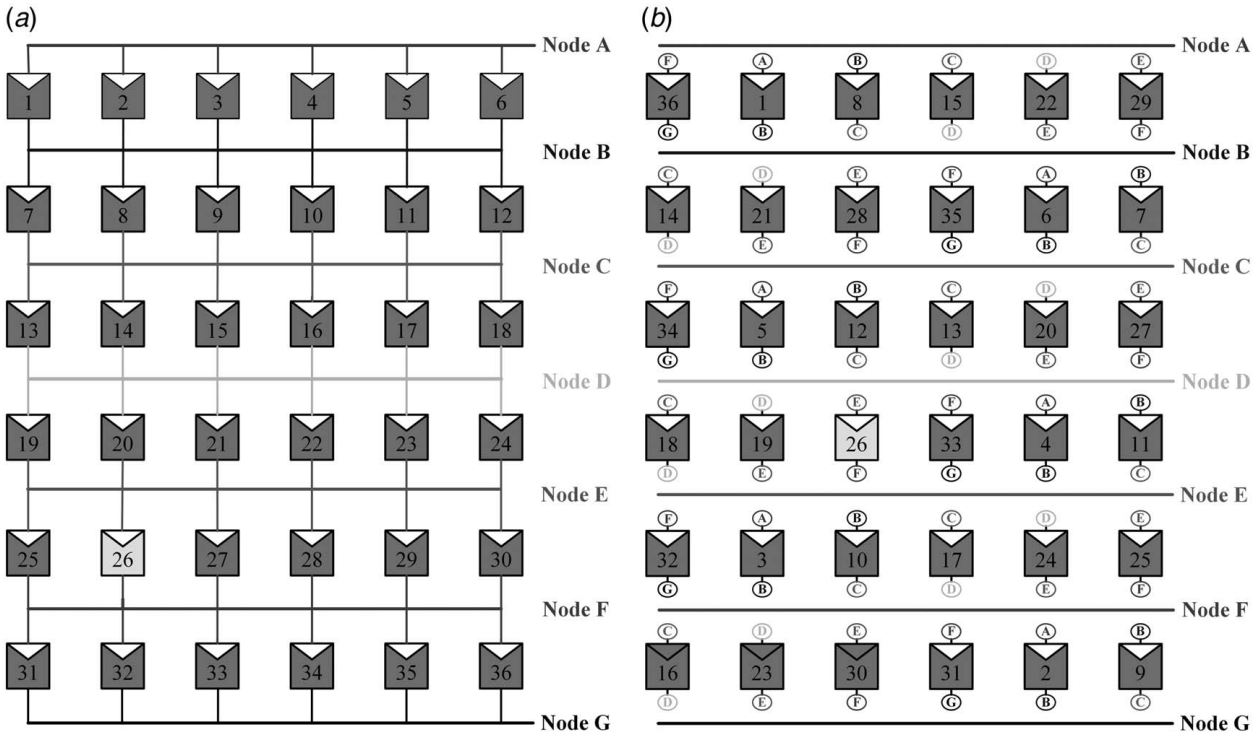

Fig. 8 Structural arrangement of PV panels in (*a*) TCT and (*b*) ACM configurations of PV array without altering electrical interconnections

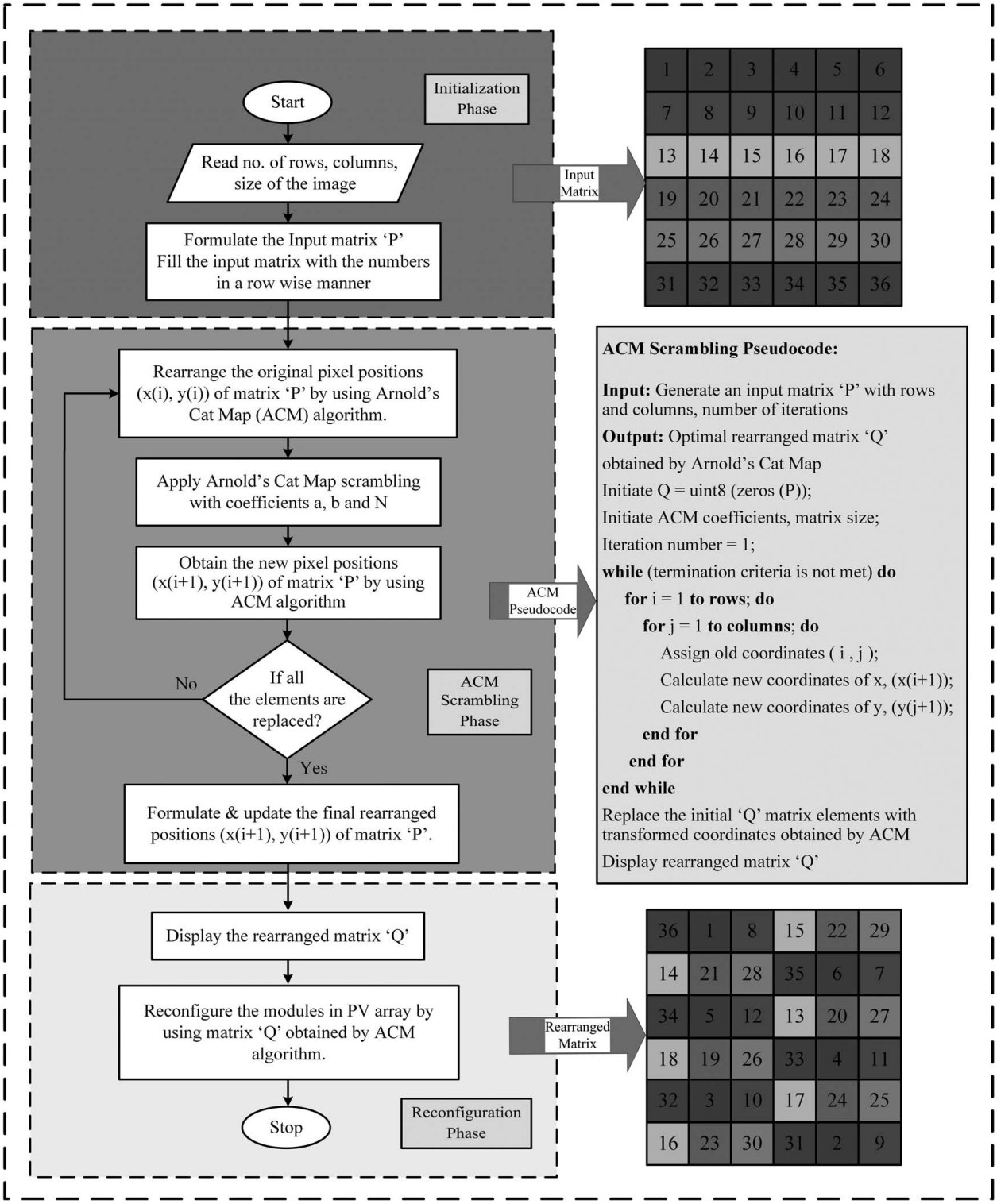

Fig. 9 Flowchart of PV array reconfiguration technique using Arnold's cat map algorithm

coordinates to new coordinates. For example, it is noted from Fig. 6 that the element "11" of original 7 × 7 matrix located in (2,4) coordinates and when applied with ACM, it is moved to (1,5) coordinates (new pixel location). Similarly, the element "12" that is located in (2,5) coordinates of the original matrix is moved to (4,3) coordinates. Likewise, all the pixel coordinates of the original matrix are effectively rearranged attaining least correlation between the adjacent pixels in the rearranged matrix.

The original 7 × 7 matrix shown in Fig. 6 has the red-colored elements numbered from 1 to 7 are placed in the same row. It is noted that the ACM rearranges all the pixels by dispersing the same-colored elements in all the rows evenly over the entire matrix, highly mitigating the correlation between adjacent pixels in a particular row. As the image comprises numerous pixels (from Fig. 7), the PV array is also composed of many solar panels connected in series and parallel to obtain the rated output. The image encryption

Table 1 Comparison of various performance parameters of a 6 × 6 PV array under various nonuniform shading conditions

Config.	GMP (W)	MM_P (W)	P_L (%)	FF	η (%)	Y_A (h/d)	C.F	P.R (%)	No. of MPPs
Case-1: Under short and broad shading pattern									
SP	3170.6	3344.1	51.33	0.376	9.60	3.407	0.198	48.67	4
TCT	3170.6	3344.1	51.33	0.376	9.60	3.407	0.210	48.67	4
OE [24]	4578.1	1936.6	29.73	0.697	13.87	4.919	0.160	70.27	3
OEP [25]	4681.8	1832.9	28.13	0.713	14.18	5.031	0.177	71.87	3
CBM [22]	4578.1	1936.6	29.73	0.697	13.87	4.919	0.199	70.27	3
ACM	4717.0	1797.7	27.59	0.774	14.29	5.068	0.218	72.41	1
Case-2: Under short and narrow shading pattern									
SP	4420.3	2094.4	32.15	0.524	13.56	4.75	0.198	67.85	3
TCT	4661.0	1853.7	28.45	0.552	14.30	5.008	0.209	71.55	3
OE [24]	4003.8	2510.9	38.54	0.474	12.29	4.302	0.179	61.46	4
OEP [25]	4220.0	2294.7	35.22	0.500	12.95	4.534	0.189	64.78	5
CBM [22]	4803.3	1711.4	26.27	0.627	14.74	5.161	0.215	73.73	5
ACM	5193.6	1321.1	20.28	0.773	15.94	5.58	0.233	79.72	1
Case-3: Under long and broad shading pattern									
SP	3524.8	2989.9	45.89	0.49	11.57	3.787	0.158	54.11	3
TCT	3563.2	2951.5	45.31	0.496	11.69	3.829	0.160	54.69	3
OE [24]	3516.3	2998.4	46.03	0.417	11.54	3.778	0.157	53.97	4
OEP [25]	3851.4	2663.3	40.88	0.456	12.64	4.138	0.172	59.12	5
CBM [22]	3563.2	2951.5	45.31	0.465	11.69	3.829	0.160	54.69	5
ACM	4134.1	2380.6	36.54	0.551	13.57	4.442	0.185	63.46	2
Case-4: Under long and narrow shading pattern									
SP	4419.5	2095.2	32.16	0.615	12.89	4.749	0.198	67.84	3
TCT	4683.5	1831.2	28.11	0.651	13.66	5.032	0.210	71.89	3
OE [24]	3579.7	2935	45.05	0.424	10.44	3.846	0.160	54.95	4
OEP [25]	3964.2	2550.5	39.15	0.507	11.56	4.260	0.177	60.85	6
CBM [22]	4444.3	2070.4	31.78	0.58	12.96	4.775	0.199	68.22	6
ACM	4871.7	1643	25.22	0.742	14.21	5.235	0.218	74.78	2

concept is applied here by considering an individual PV panel as a pixel of an image, and the whole PV array as an image consisting of pixels. The panels in the array are configured based on the rearranged matrix pattern obtained by ACM to disperse the shade evenly over the array.

4.3 Evolution of Arnold's Cat Map-Based Photovoltaic Array Reconfiguration. To improve the array output under shading, PV panels are optimally interconnected in some predefined configurations. The novel ACM approach is the highly suitable and appropriate solution that can be employed in the optimal array reconfiguration of TCT as it disperses the elements uniformly in all the rows resulting in even shade dispersal over the entire without disturbing the electrical circuitry. This doesn't induce any difference in its electrical properties while diminishing the shading impact. The PV panels in TCT as are physically relocated based on rearranged ACM matrix and the structural difference in the arrangement between conventional TCT and the proposed ACM arrangement with new locations of the panels in an array is shown in Fig. 8.

All the panels are denoted with the nodes on either side of the PV panels, which symbolizes that they are electrically interconnected to the same row. From Fig. 8(*a*), it is noted that the panel number "26" is in the fifth row and the second column in the conventional TCT, and (based on rearranged matrix shown in Fig. 9) this panel is physically relocated to the fourth row and the third column, i.e., in between Node-E and Node-F as shown in Fig. 8(*b*). Similarly, all the panels are optimally reconfigured based on the rearranged ACM matrix to disperse the shade evenly. Suppose if the first row of the reconfigured array with panel numbers 36, 1, 8, 15, 22, and 29 are shaded and as these panels are physically located in the first row but electrically connected to distinct rows of an array, the shade is equally distributed over the entire array equalizing the irradiation in rows. In consequence, the proposed image encryption-based panel reconfiguration strategy maximizes the energy harvest.

5 Various Performance Indices

To confirm the superior performance of proposed technique the system has been extensively investigated with global maximum power (GMP), fill factor (FF) [26], power loss (P_L), efficiency (η), mismatch power (MM_P) [26], performance ratio (PR), capacity factor (CF) [14], array yield (Y_A) [14].

5.1 Fill Factor. It is the measure of the conversion efficiency of a PV module [27]. FF is determined as follows:

$$\mathrm{FF} = \frac{V_{\mathrm{MPP}} \times I_{\mathrm{MPP}}}{V_{\mathrm{oc}} \times I_{\mathrm{sc}}}$$

5.2 Power Loss (%). It is the ratio of difference between GMP obtained at shaded (GMP_{PS}) and unshaded conditions to the GMP obtained at unshaded conditions (GMP_{STC}).

$$P_L(\%) = \frac{\mathrm{GMP_{STC}} - \mathrm{GMP_{PS}}}{\mathrm{GMP_{STC}}}$$

5.3 Efficiency (%). The efficiency (η) of PV array is defined as the ratio of array output to the amount of incident solar irradiation delivered by the sun [26]. It is given by

$$\eta(\%) = \frac{V_{\mathrm{MPP}} \times I_{\mathrm{MPP}}}{G \times A}$$

where "G" is the solar irradiation (W/m^2) and A is the panel area (1425 mm × 990 mm for KG200GT panel).

5.4 Array Yield (h/d). The array yield (Y_A) signifies the number of hours required by PV array to produce the energy at its nominal capacity [14]. It is calculated by dividing the finally obtained DC energy of the array ($E_{dc,array}$) to the rated capacity of

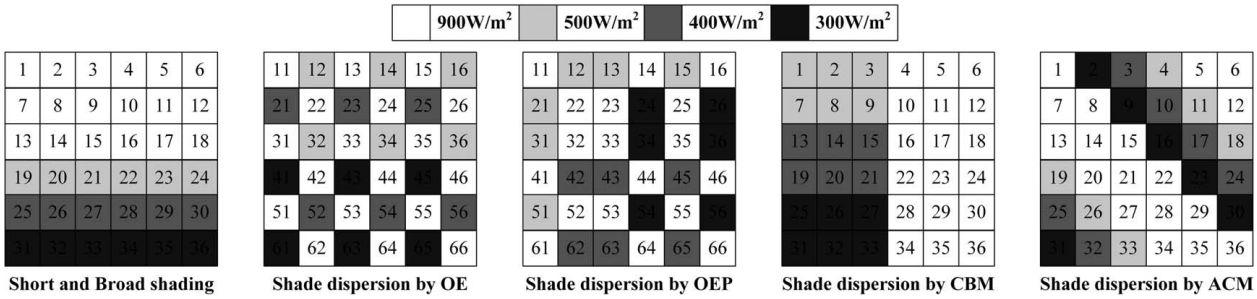

Fig. 10 SB shading and the corresponding shade dispersions with OE, OEP, CBM, and ACM

Table 2 Theoretical computations of various configurations under SB shading

Current, I_{Ri} (A); voltage, V_m (V); power, P_m (W)

TCT configuration				OE configuration [24]				OEP configuration [25]			
Row	I_{Ri}	V_m	P_m	Row	I_{Ri}	V_m	P_m	Row	I_{Ri}	V_m	P_m
R_6	1.8 I_m	6 V_m	10.8 V_mI_m	R_4	3.6 I_m	6 V_m	21.6 V_mI_m	R_2	3.8 I_m	6 V_m	22.8 V_mI_m
R_5	2.4 I_m	5 V_m	12 V_mI_m	R_6	—	—	—	R_3	—	—	—
R_4	3 I_m	4 V_m	12 V_mI_m	R_2	3.9 I_m	4 V_m	15.6 V_mI_m	R_5	—	—	—
R_1	5.4 I_m	3 V_m	16.2 V_mI_m	R_5	—	—	—	R_4	3.9 I_m	3 V_m	11.7 V_mI_m
R_2	—	—	—	R_1	4.2 I_m	2 V_m	8.4 V_mI_m	R_6	—	—	—
R_3	—	—	—	R_3	—	—	—	R_3	4.2 I_m	V_m	4.2 V_mI_m

CBM configuration [22]				ACM configuration			
Row	I_{Ri}	V_m	P_m	Row	I_{Ri}	V_m	P_m
R_5	3.6 I_m	6 V_m	21.6 V_mI_m	R_1	3.9 I_m	6 V_m	23.4 V_mI_m
R_6	—	—	—	R_2	—	—	—
R_3	3.9 I_m	4 V_m	15.6 V_mI_m	R_3	—	—	—
R_4	—	—	—	R_4	—	—	—
R_1	4.2 I_m	2 V_m	8.4 V_mI_m	R_5	—	—	—
R_2	—	—	—	R_6	—	—	—

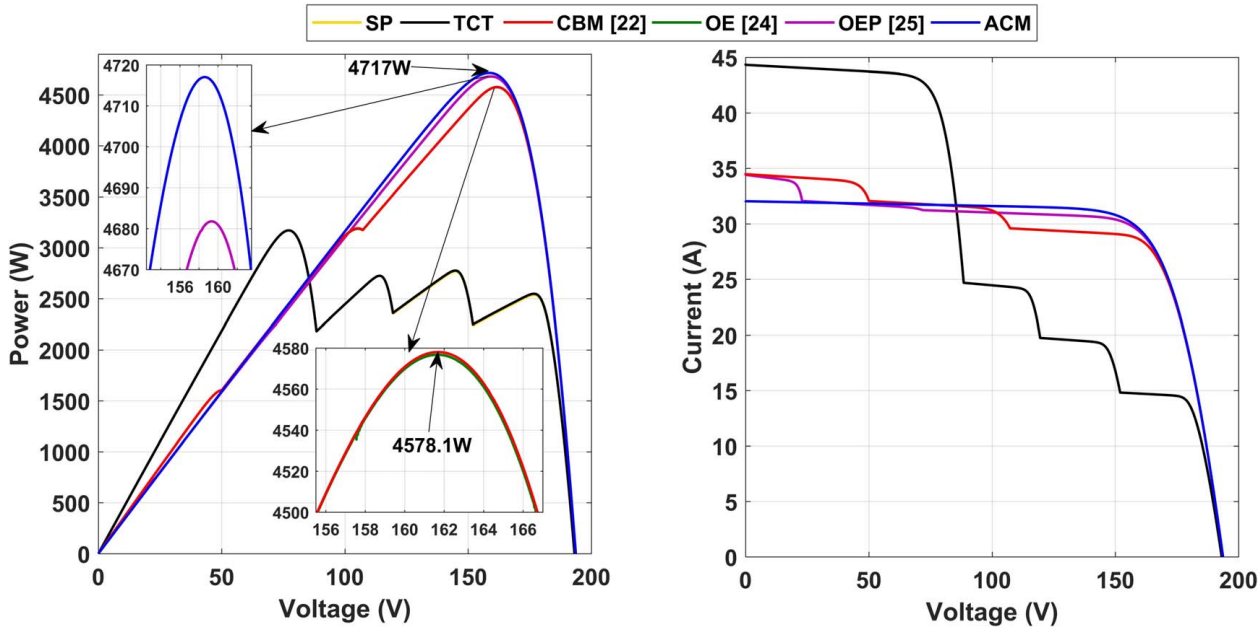

Fig. 11 Power–voltage and current–voltage characteristics under SB shading pattern (at $T = 25$ °C)

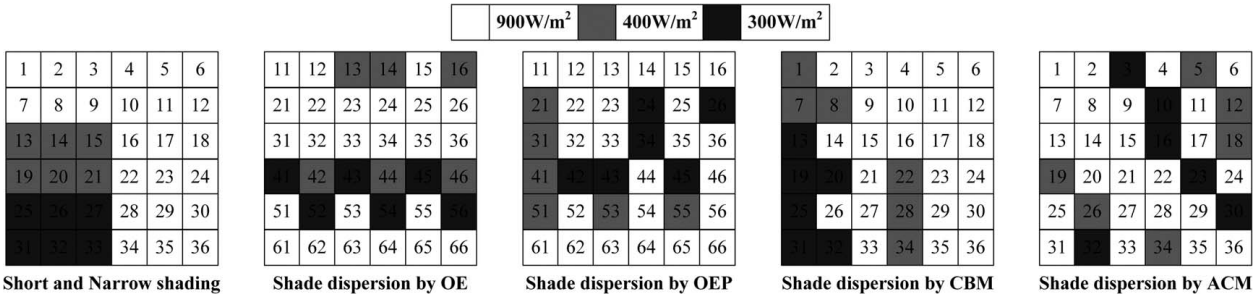

Fig. 12 SN shading and the corresponding shade dispersions with OE, OEP, CBM, and ACM

Table 3 Theoretical computations of various configurations under SN shading

Current, I_{Ri} (A); voltage, V_m (V); power, P_m (W)

TCT configuration				OE configuration [24]				OEP configuration [25]			
Row	I_{Ri}	V_m	P_m	Row	I_{Ri}	V_m	P_m	Row	I_{Ri}	V_m	P_m
R_5	3.6 I_m	6 V_m	21.6 V_mI_m	R_4	2.1 I_m	6 V_m	12.6 V_mI_m	R_4	3.1 I_m	6 V_m	18.6 V_mI_m
R_6	—	—	—	R_5	3.6 I_m	5 V_m	18 V_mI_m	R_2	3.7 I_m	5 V_m	18.5 V_mI_m
R_3	3.9 I_m	4 V_m	15.6 V_mI_m	R_1	3.9 I_m	4 V_m	15.6 V_mI_m	R_5	3.9 I_m	4 V_m	15.6 V_mI_m
R_4	—	—	—	R_2	5.4 I_m	3 V_m	16.2 V_mI_m	R_3	4.3 I_m	3 V_m	12.9 V_mI_m
R_1	5.4 I_m	2 V_m	10.8 V_mI_m	R_3	—	—	—	R_1	5.4 I_m	2 V_m	10.8 V_mI_m
R_2	—	—	—	R_6	—	—	—	R_6	—	—	—

CBM configuration [22]				ACM configuration			
Row	I_{Ri}	V_m	P_m	Row	I_{Ri}	V_m	P_m
R_4	3.7 I_m	6 V_m	22.2 V_mI_m	R_1	4.3 I_m	6 V_m	25.8 V_mI_m
R_6	—	—	—	R_2	—	—	—
R_5	4.3 I_m	4 V_m	17.2 V_mI_m	R_3	—	—	—
R_2	4.4 I_m	3 V_m	13.2 V_mI_m	R_4	—	—	—
R_3	4.8 I_m	2 V_m	9.6 V_mI_m	R_5	—	—	—
R_1	4.9 I_m	V_m	4.9 V_mI_m	R_6	—	—	—

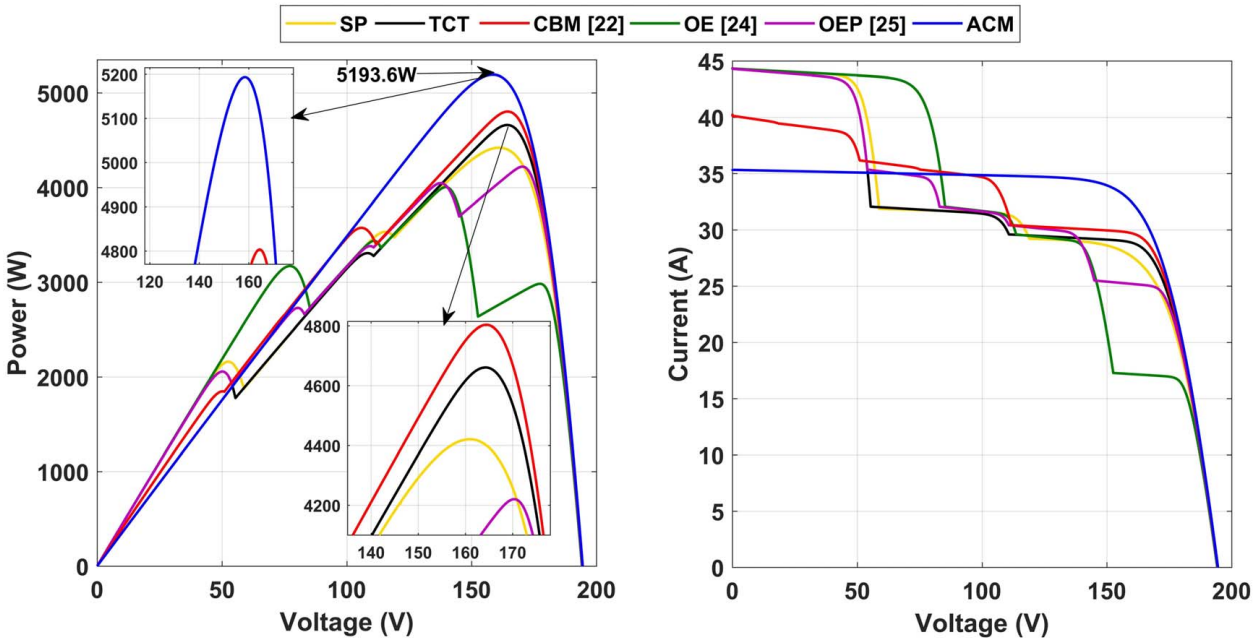

Fig. 13 Power–voltage and current–voltage characteristics under SN shading pattern (at $T = 25$ °C)

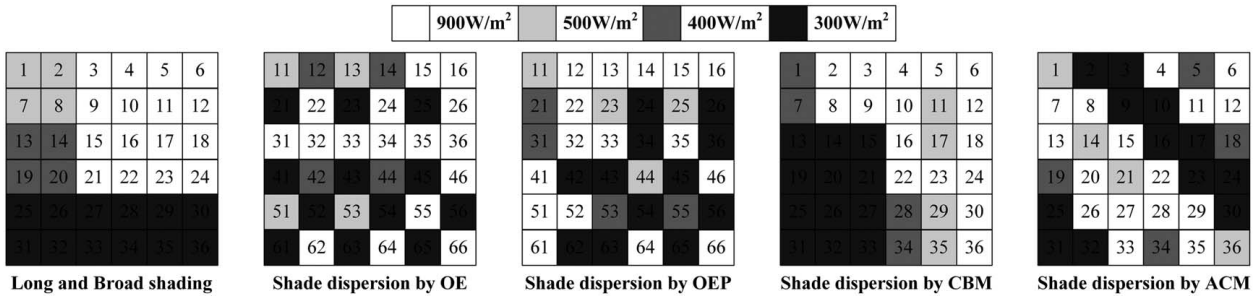

Fig. 14 LB shading and the corresponding shade dispersions with OE, OEP, CBM, and ACM

Table 4 Theoretical computations of various configurations under LB shading

Current, I_{Ri} (A); voltage, V_m (V); power, P_m (W)

TCT configuration				OE configuration [24]				OEP configuration [25]			
Row	I_{Ri}	V_m	P_m	Row	I_{Ri}	V_m	P_m	Row	I_{Ri}	V_m	P_m
R_5	1.8 I_m	6 V_m	10.8 V_mI_m	R_4	2.6 I_m	6 V_m	15.6 V_mI_m	R_2	2.9 I_m	6 V_m	17.4 V_mI_m
R_6	—	—	—	R_5	2.8 I_m	5 V_m	14 V_mI_m	R_4	3.2 I_m	5 V_m	16 V_mI_m
R_3	4.4 I_m	4 V_m	17.6 V_mI_m	R_1	3.6 I_m	4 V_m	14.4 V_mI_m	R_5	—	—	—
R_4	—	—	—	R_2	—	—	—	R_6	3.6 I_m	3 V_m	10.8 V_mI_m
R_1	4.6 I_m	2 V_m	9.2 V_mI_m	R_6	—	—	—	R_3	3.7 I_m	2 V_m	7.4 V_mI_m
R_2	—	—	—	R_3	5.4 I_m	V_m	5.4 V_mI_m	R_1	5 I_m	V_m	5 V_mI_m

CBM configuration [22]				ACM configuration			
Row	I_{Ri}	V_m	P_m	Row	I_{Ri}	V_m	P_m
R_5	2.7 I_m	6 V_m	16.2 V_mI_m	R_1	3.3 I_m	6 V_m	19.8 V_mI_m
R_6	—	—	—	R_3	—	—	—
R_3	3.2 I_m	4 V_m	12.8 V_mI_m	R_4	—	—	—
R_4	3.6 I_m	3 V_m	10.8 V_mI_m	R_6	—	—	—
R_2	4.5 I_m	2 V_m	9 V_mI_m	R_2	4.2 I_m	2 V_m	8.4 V_mI_m
R_1	4.9 I_m	1 V_m	4.9 V_mI_m	R_5	—	—	—

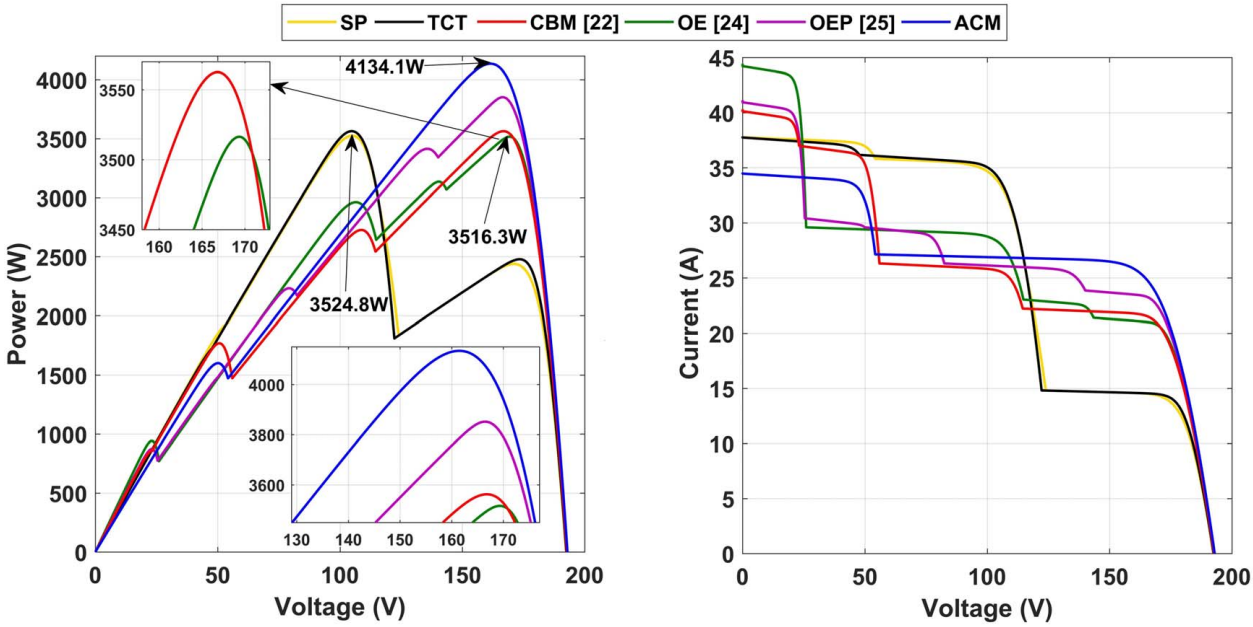

Fig. 15 Power–voltage and current–voltage characteristics under LB shading pattern (at $T = 25$ °C)

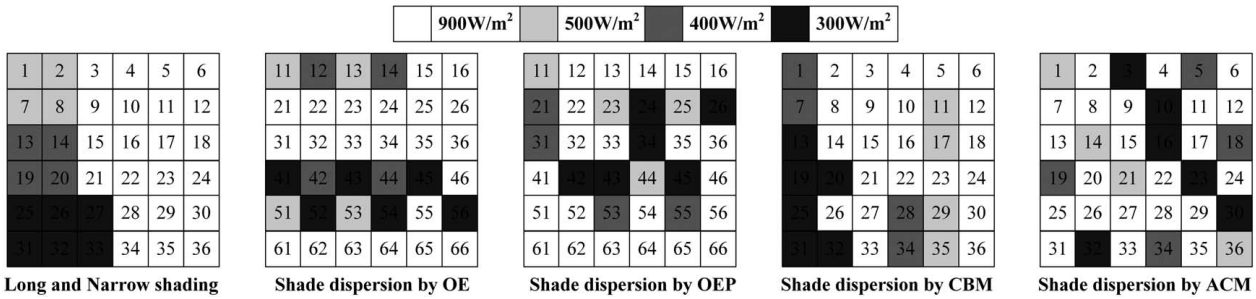

Fig. 16 LN shading and the corresponding shade dispersions with OE, OEP, CBM, and ACM

Table 5 Theoretical computations of various configurations under LN shading

Current, I_{Ri} (A); voltage, V_m (V); power, P_m (W)

TCT configuration				OE configuration [24]				OEP configuration [25]			
Row	I_{Ri}	V_m	P_m	Row	I_{Ri}	V_m	P_m	Row	I_{Ri}	V_m	P_m
R_5	3.6 I_m	6 V_m	21.6 V_mI_m	R_4	2.6 I_m	6 V_m	15.6 V_mI_m	R_2	2.9 I_m	6 V_m	17.4 V_mI_m
R_6	—	—	—	R_5	2.8 I_m	5 V_m	14 V_mI_m	R_4	3.2 I_m	5 V_m	16 V_mI_m
R_3	4.4 I_m	4 V_m	17.6 V_mI_m	R_1	3.6 I_m	4 V_m	14.4 V_mI_m	R_3	4.3 I_m	4 V_m	17.2 V_mI_m
R_4	—	—	—	R_2	5.4 I_m	3 V_m	16.2 V_mI_m	R_5	4.4 I_m	3 V_m	13.2 V_mI_m
R_1	4.6 I_m	2 V_m	9.2 V_mI_m	R_3	—	—	—	R_1	5 I_m	2 V_m	10 V_mI_m
R_2	—	—	—	R_6	—	—	—	R_6	5.4 I_m	V_m	5.4 V_mI_m

CBM configuration [22]				ACM configuration			
Row	I_{Ri}	V_m	P_m	Row	I_{Ri}	V_m	P_m
R_6	3.3 I_m	6 V_m	19.8 V_mI_m	R_1	3.9 I_m	6 V_m	23.4 V_mI_m
R_5	3.9 I_m	5 V_m	19.5 V_mI_m	R_3	—	—	—
R_4	4.2 I_m	4 V_m	16.8 V_mI_m	R_4	—	—	—
R_3	4.4 I_m	3 V_m	13.2 V_mI_m	R_6	—	—	—
R_2	4.5 I_m	2 V_m	9 V_mI_m	R_2	4.8 I_m	2 V_m	9.6 V_mI_m
R_1	4.9 I_m	V_m	4.9 V_mI_m	R_5	—	—	—

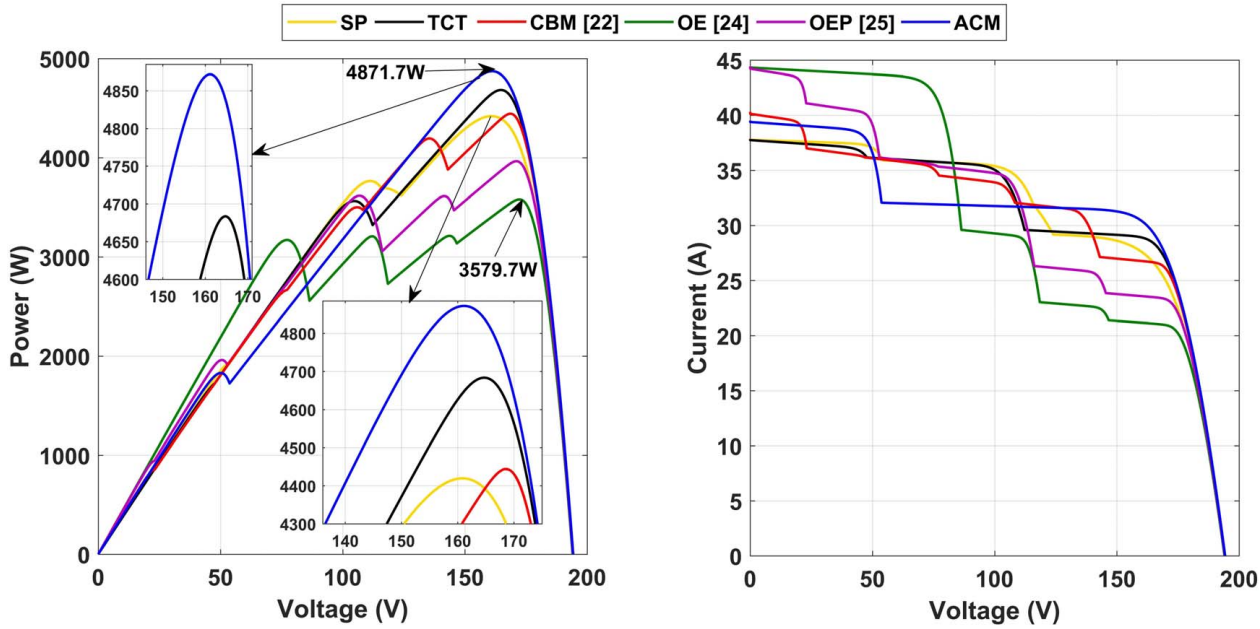

Fig. 17 Power–voltage and current–voltage characteristics under LN shading pattern (at $T = 25$ °C)

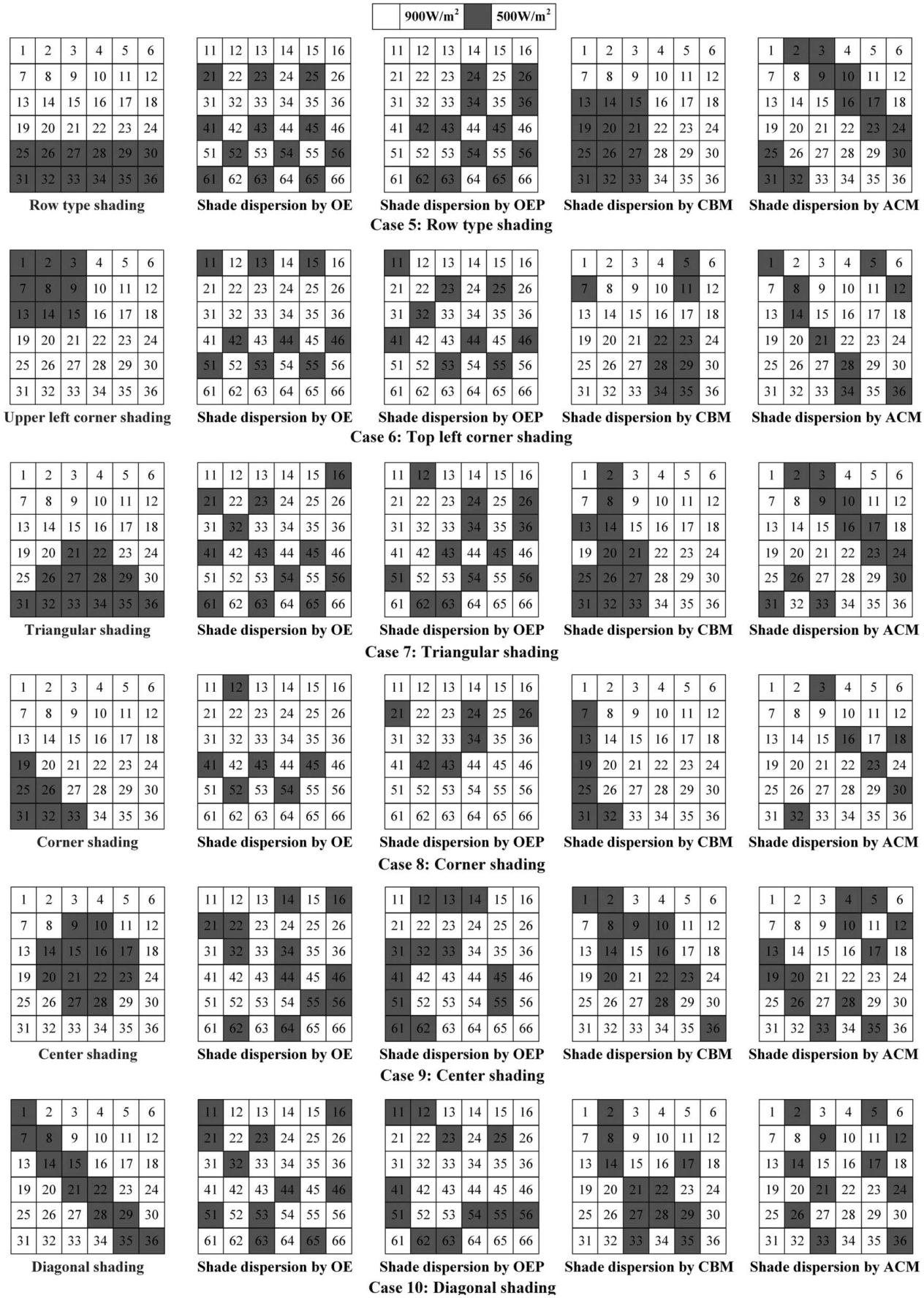

Fig. 18 Distinct uniform shading cases 6 × 6 PV array and their corresponding shade dispersions with OE, OEP, CBM, and ACM techniques

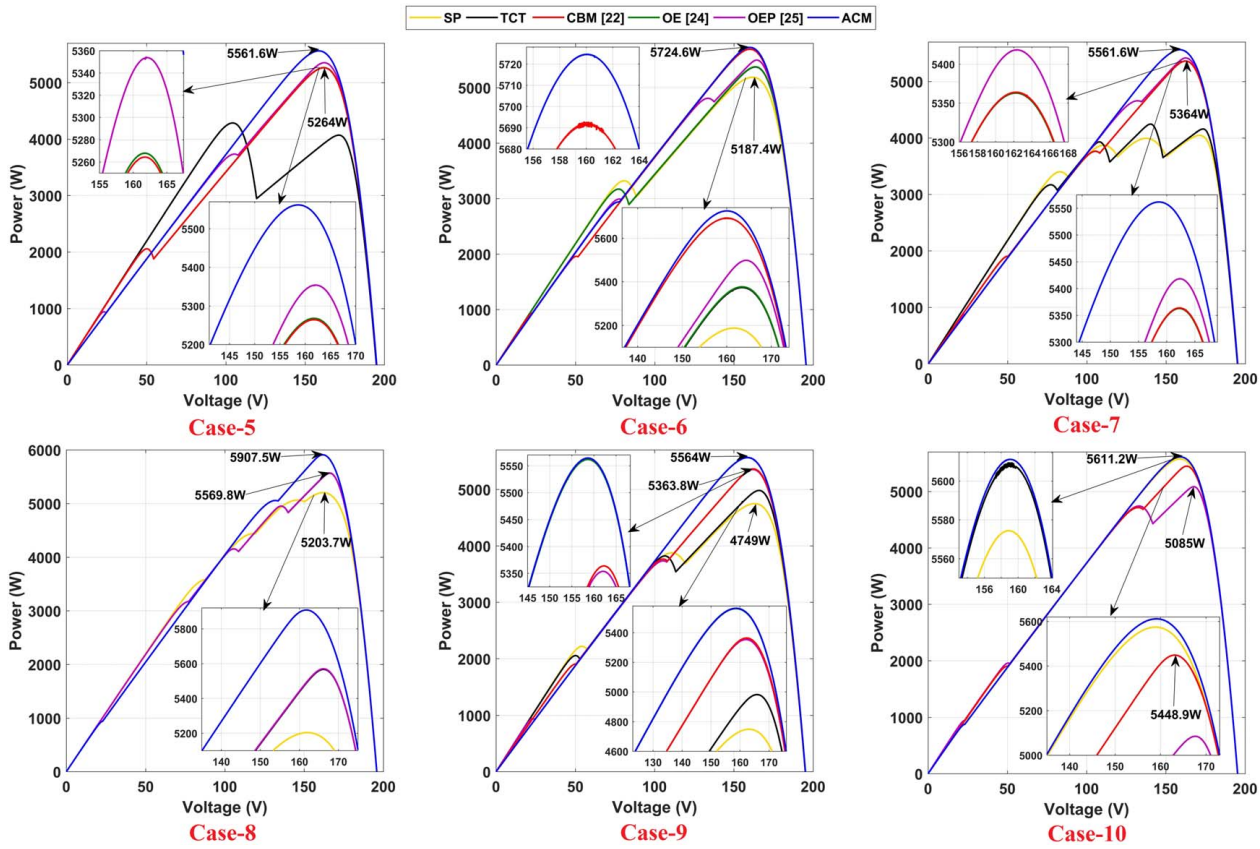

Fig. 19 Power–voltage characteristics of 6 × 6 array under case-5 to case-10 shading (at $T = 25$ °C)

the PV array.

$$Y_A(h/d) = \frac{E_{dc,array}}{P_{rated}}$$

6 Results and Discussions

To verify the compatibility and effectiveness of the proposed ACM technique, an even-sized 6 × 6 symmetrical PV array is tested under various nonuniform and uniform shading cases. The theoretical computations of the PV array with TCT, OE, OEP, CBM, and ACM configurations under various nonuniform shading cases are presented in the subsequent sections. To justify these theoretical computations, MATLAB-based simulations are also conducted. For analysis, a KG200GT-200W panel is considered at STC (900 W/m^2, 25 °C). By using the aforementioned performance indices, the functionality of the proposed reconfiguration technique has been analyzed.

6.1 Analysis of 6 × 6 Photovoltaic Array Under Nonuniform Shading Conditions.

During nonuniform shading, the unshaded modules of an even symmetrical 6 × 6 PV array receive the irradiation of 900 W/m^2 and the shaded modules receive 500 W/m^2, 400 W/m^2, and 300 W/m^2, respectively. The comparison of various performance parameters of a 6 × 6 PV array under various nonuniform shading conditions is given in Table 1.

Table 6 GMP of various configurations of 6 × 6 array under various uniform shading conditions

Config.	Case-5	Case-6	Case-7	Case-8	Case-9	Case-10
SP	4285.3	5187.4	4046.5	5203.7	4748.8	5574.4
TCT	4285.3	5373.1	4244.8	5566.6	4981.8	5611.2
OE [24]	5267.9	5376.5	5363.8	5569.9	5561.6	5611.2
OEP [25]	5354.2	5498.1	5418.3	5569.8	5353.8	5085.0
CBM [22]	5264.4	5692.6	5363.9	5907.7	5363.8	5448.9
ACM	5561.6	5724.6	5561.6	5907.7	5564.0	5611.2

6.1.1 Case-1: Under Short and Broad (SB) Shading. During this case, the shading pattern is short and broad typed as shown in Fig. 10. It is observed from Fig.10 that the ACM disperses the shade uniformly over the entire array through effective reconfiguration leading to zero mismatches in row currents thereby exhibiting only one power peak (from Table 2). Whereas, the TCT, OE, OEP, and CBM configurations exhibit a broad range of row current variation respectively yielding three to four MPPs due to their poor shade dispersal as shown in Fig. 10 Amongst all techniques, TCT yields the least GMP of 16.2 V_mI_m and ACM yields the highest GMP of 23.4 V_mI_m. From the array PV and IV characteristic curves shown in Fig. 11, it is noted that the respective GMP obtained by OE, OEP, CBM, and ACM configurations under the SB shading is 4578.1 W, 4681.8 W, 4578.1 W, and 4717.0 W which is 44.40%, 47.67%, 44.40%, and 48.78% more compared to TCT. Besides yielding the highest GMP, the proposed ACM technique reduces the LMPPs as it reduces the total bypasses in the array and exhibits smoother array PV and IV characteristics. Furthermore, the effectiveness is also manifested in the enhanced values of other performance metrics as noted from Table 1.

6.1.2 Case-2: Under Short and Narrow (SN) Shading. During this case, a short and narrow portion of the 6 × 6 PV array is experienced with low irradiation levels while the remaining part of the array gets maximum irradiation of 900 W/m^2 as shown in Fig. 12.

During SN shading, on contrary to existing SP, TCT, OEM OEP, CBM, the proposed ACM uniformly disperses the shade over the entire array exhibiting only one power peak with zero mismatches

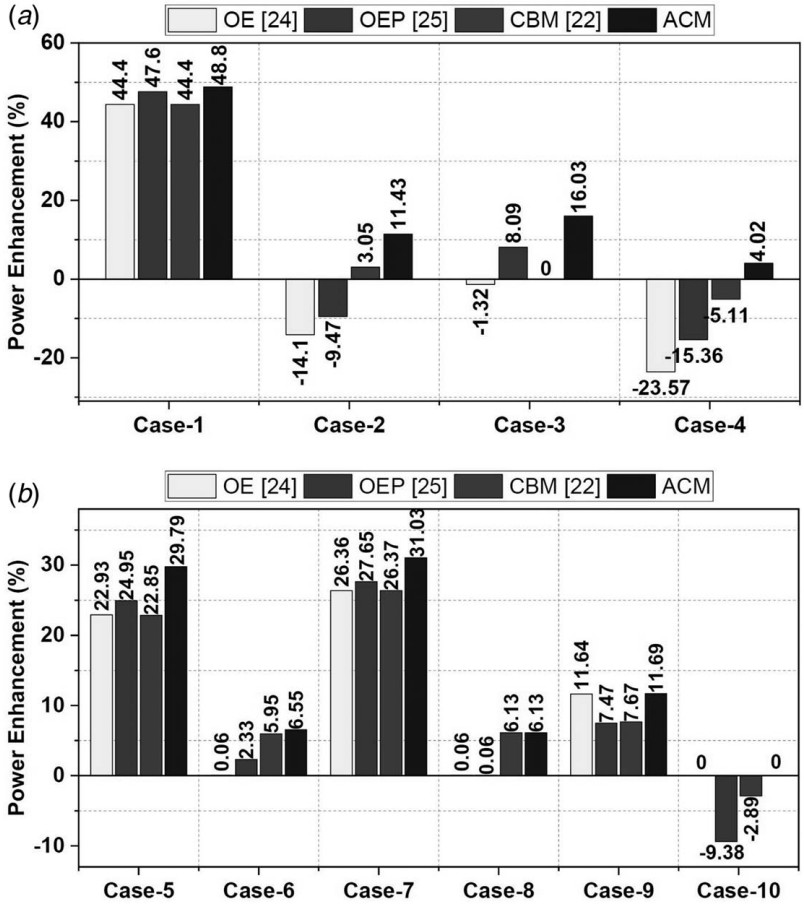

Fig. 20 GMP enhancement of a 6 × 6 array under (*a*) nonuniform and (*b*) uniform shading (at $T = 25$ °C)

and the highest GMP of 25.8 V_mI_m. Despite their compatibility to all array sizes, the indiscriminate and poor shade dispersal of the existing OE and OEP resulted in inferior performance even compared to conventional TCT. The power enhancement with the CBM is also not so significant which is only from 21.6 V_mI_m to 22.2 V_mI_m (theoretically) and 3.05% experimentally. The CBM technique, in addition to its low power enhancement, exhibits the most unsatisfactory results with the row current bypassing taking place at each row.

The OE and OEP techniques, besides yielding inferior output and exhibiting a broad range of row current variation, generate four to six power peaks (from Table 3 and Fig. 13). Due to the zero-mismatch obtained by the ACM technique, there is a significant improvement in the array characteristics as shown in Fig. 13. The GMP obtained by SP, TCT, OE, OEP, CBM, and ACM is 4420.3 W, 4661.0 W, 4003.8 W, 4220.0 W, 4803.3 W, and 5193.6 W, respectively. The proposed ACM yields the highest GMP enhancing the output by 11.43%, followed by CBM (3.05%). Hence, the proposed ACM technique not only offers a peerless performance but also eliminates the drawback of the OE, OEP, and CBM techniques.

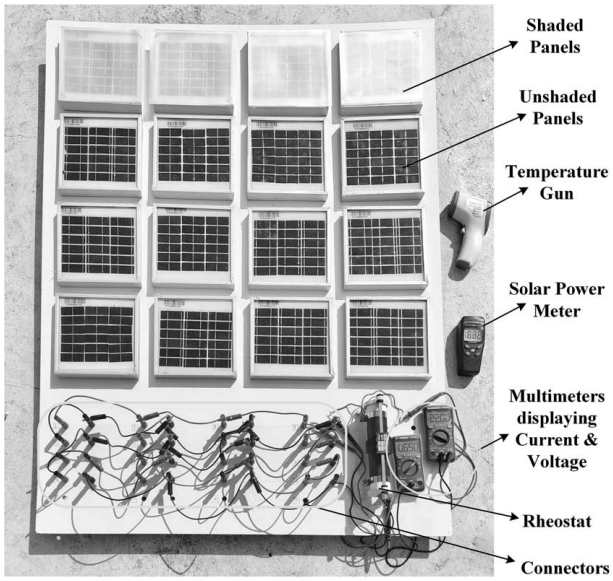

Fig. 21 Experimental setup of a 4 × 4 array reconfiguration system

6.1.3 Case-3: Under Long and Broad (LB) Shading. Under this shading condition, many panels encompassing a large part of rows and columns in a PV array are shaded as shown in Fig. 14.

It is noted from Table 4 that the proposed ACM yields the highest GMP of 19.8 V_mI_m offering a narrow range of row currents varying from 3.3 I_m to 4.2 I_m thereby yielding smooth characteristics as shown in Fig. 15. Whereas the TCT, OE, OEP, and CBM configurations offer a broad range of row currents. Moreover, all these techniques give the most unsatisfactory outcomes with the row current bypasses taking place at many rows. The ACM configuration delivers an unprecedented GMP of 4134.1 W which is 16.03% more, while on contrary, the CBM and TCT configurations perform on par with each other delivering a GMP of 3563.2 W. Due to poor shade dispersion, the OE yields only 3516.3 W which is 1.32%

Table 7 Simulation results of 4 × 4 PV array under shading cases 1–11

Dynamic shading	Power output (W)					Static shading	Power output (W)				
	TCT	OE	OEP	CBM	ACM		TCT	OE	OEP	CBM	ACM
Case-1	14.51	24.48	24.85	28.24	28.24	Case-7	24.48	24.85	24.85	24.48	28.24
Case-2	14.51	24.48	24.85	24.48	28.24	Case-8	13.01	22.09	22.09	17.85	22.09
Case-3	14.51	24.48	24.85	24.48	28.24	Case-9	18.45	19.32	19.32	23.77	23.77
Case-4	28.70	25.03	25.03	25.03	28.70	Case-10	16.6	23.78	23.78	23.78	23.78
Case-5	28.24	24.48	24.48	24.48	28.24	Case-11	23.78	23.78	19.317	19.317	23.78
Case-6	28.70	28.70	25.03	25.03	28.70						

Table 8 GMP of various configurations of 6 × 9 PV array under distinct shading conditions

Config.	Case-1	Case-2	Case-3	Case-4	Case-5	Case-6
TCT	8100.0	6428.0	8818.9	8018.8	7198.4	7671.2
OE [24]	8130.2	7777.9	8436.0	8045.9	8285.1	6886.1
OEP [25]	8714.4	8182.2	7697.0	7652.5	8278.8	7419.1
ACM	9006.4	8195.1	8818.9	8333.1	8376.5	8080.9

less than TCT. Followed by ACM, OEP enhances the GMP by 8.09% which is 3851.4 W. The ACM technique offers the least mismatch loss, highest FF, efficiency, and array yield.

6.1.4 Case-4: Under Long and Narrow (LN) Shading. For analyzing the practical shading scenario, a substantial length of the array is considered to be shaded as shown in Fig. 16.

It is noted from Table 5 that the proposed ACM offers superior performance exhibiting only two bypasses with the highest GMP of 23.4 $V_m I_m$ and narrow row current variation ranging from 3.9 I_m to 4.8 I_m. Under this shading case, all the existing OE, OEP, and CBM techniques fail to disperse the shade uniformly thereby offering highly inferior performance yielding the highest row mismatch, numerous MPPs, and bypasses (from Table 5 and Fig. 17). The efficacy of the proposed ACM technique in generating highest GMP is once again proved in yielding not only the highest output power but also reduced bypasses which helps in attaining the smoother array PV and IV characteristics which are shown in Fig. 17. The respective GMP obtained by SP, TCT, OE, OEP, CBM, and ACM configurations under the LN pattern is 4419.5 W, 4683.5 W, 3579.7 W, 3964.2 W, 4444.3 W, and 4871.7 W. The ACM technique enhances the output by 4.02%, while the existing SP, OE, OEP, and CBM exhibit inferior performance lowering the output by 5.64%, 23.57%, 15.36%, and 5.11%, respectively.

6.2 Analysis of 6 × 6 Photovoltaic Array Under Various Uniform Shading Patterns. The proposed ACM configuration is further analyzed under six distinct uniform shadowing conditions where all the shaded panels are considered to receive equal irradiation. The various uniform shading cases considered for the analysis are row-type shading, upper-left corner shading, triangular-shading, corner shading, center shading, and diagonal shading. During uniform shading, the shaded and unshaded modules are considered to receive 500 W/m^2 and 900 W/m^2, respectively. Various uniform shading cases and their corresponding shade dispersion with OE, OEP, CBM, and ACM techniques are shown in Fig. 18.

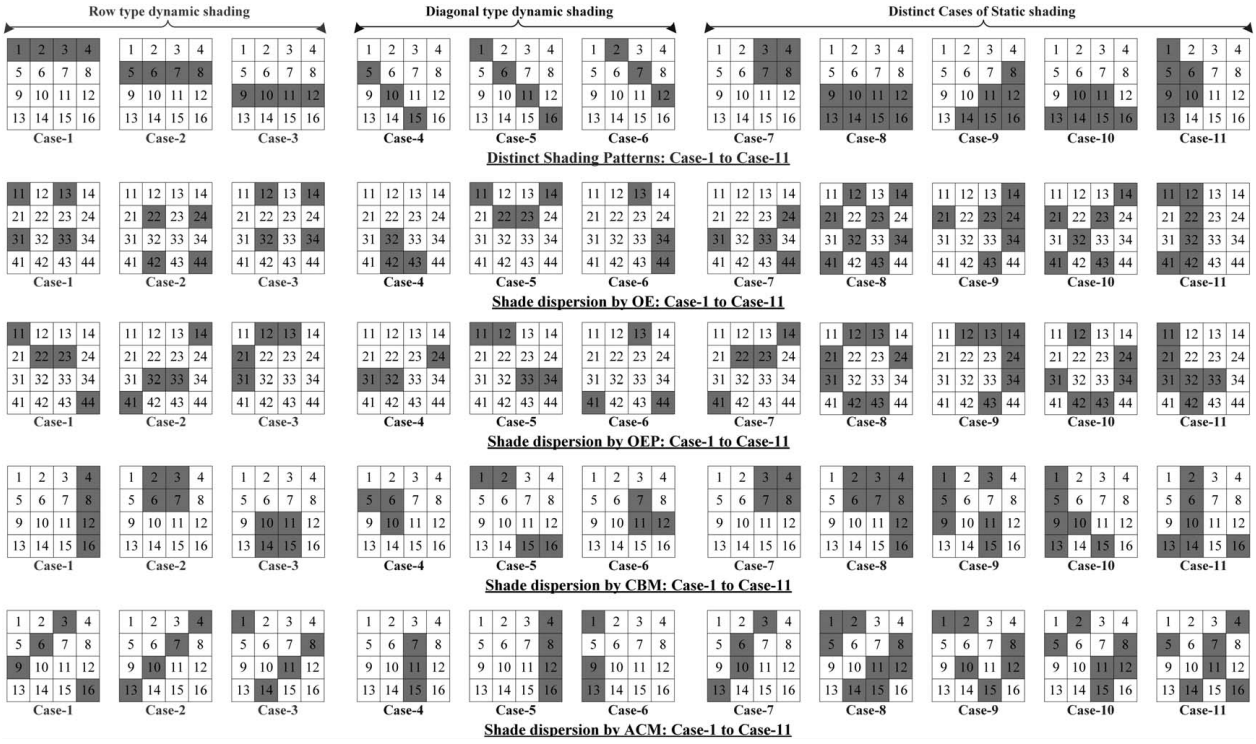

Fig. 22 Distinct dynamic and static shading cases and their shade dispersion by OE, OEP, CBM, and ACM techniques

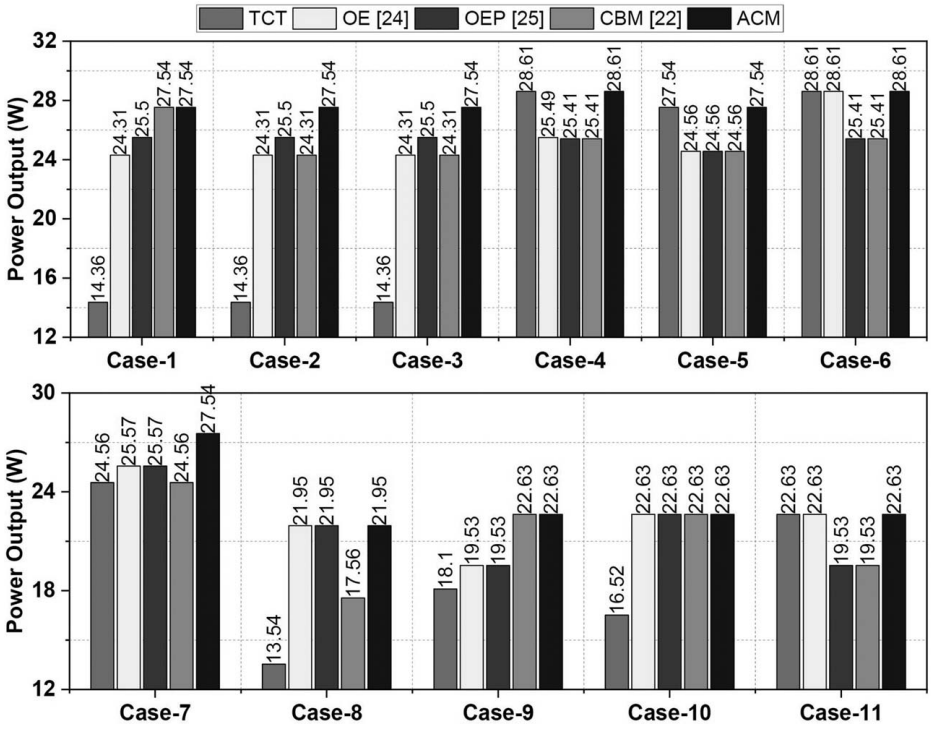

Fig. 23 Experimental results: power output under dynamic shading (case-1 to case-6) and static shading (case-7 to case-11) conditions (at $T = 29$ °C)

It is evident from Fig. 18 that the effective and uniform shade dispersion over the entire array is achieved with the proposed ACM when compared to existing OE, OEP, and CBM techniques. The array PV characteristic curves under various cases of uniform shading are shown in Fig. 19. It is noted from Fig. 19 and Table 6 that the GMP produced by ACM configuration is the highest during all the PS patterns exhibiting the least number of bypasses and MPPs with the lowest mismatch. The proposed ACM enhances the output by 29.79%, 6.55%, 31.03%, 6.13%, 11.69% during cases 5–9, respectively. The respective GMP enhancement of a 6×6 array under nonuniform and uniform shading cases is shown in Figs. 20(*a*) and 20(*b*).

6.3 Experimental Validation of Proposed Reconfiguration Scheme. To demonstrate the effectiveness of the proposed configuration in a real-time scenario, an experimental prototype model of a 4×4 reconfiguration system is developed as shown in Fig. 21. The developed prototype model consists of sixteen 3-W PV panels configured in OE, OEP, CBM, and the proposed ACM configurations by means of banana connectors as shown in the experimental setup.

The array is connected to (50 Ω, 2 A) variable rheostat which is adjusted to extract maximum power from the PV array. The technical specifications of a 3-W PV panel are shown in the Appendix (Table 9). The experimental analysis is conducted out in real-time outdoor conditions (during a noonday on December 17, 2021). The artificial shading patterns are created using some thick transparent sheets that limit the incident light from sun. The solar irradiation is measured by the solar power meter and the operating temperature of panels is measured by a temperature gun. During experimentation, the operating temperature is found to be around 29 °C and the unshaded and shaded panels receive the solar irradiation of 700 W/m^2 and 250 W/m^2 approximately.

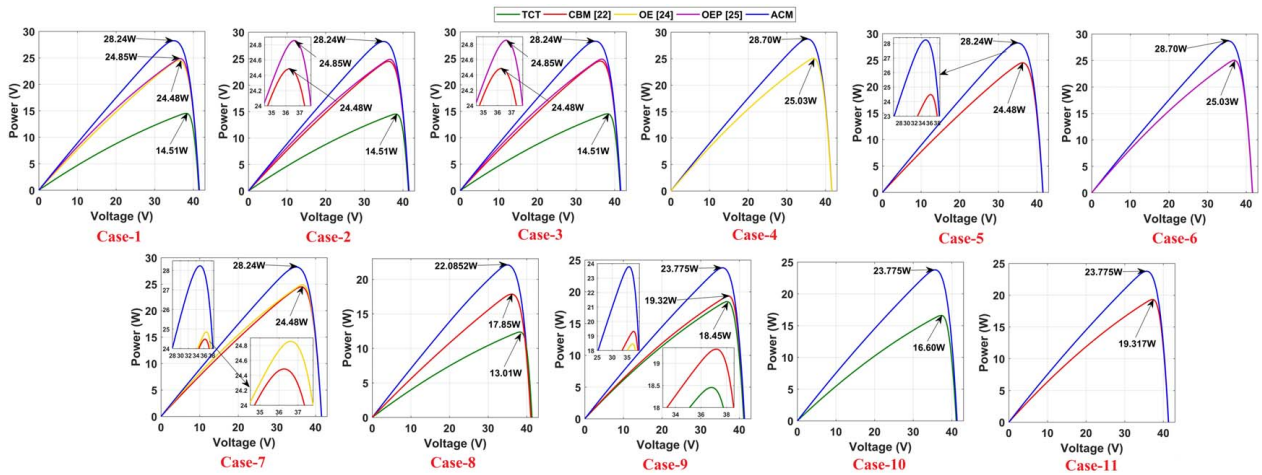

Fig. 24 Simulation results: power–voltage characteristics under shading case-1 to case-11 (at $T = 29$ °C)

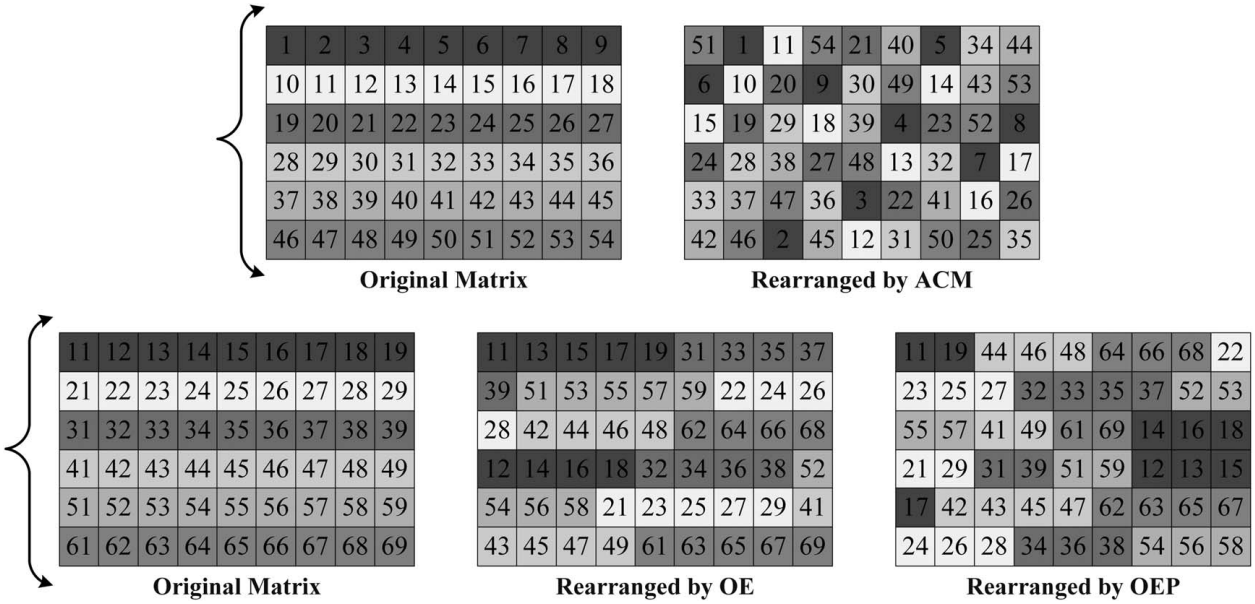

Fig. 25 Original 6 × 9 matrix and the corresponding reconfigured matrix obtained by OE, OEP, and ACM

The system is tested and validated under both dynamic and static shading conditions as shown in Fig. 22. The dynamic shading can be due to the movement of clouds, moving shade due to long poles or towers, etc., as it passes over the array. Two distinct groups of continuously moving shade covering PV array over the time such as row-type shading group and diagonal shading group is considered from case-1 to 3 and case-4 to 6, respectively. Some of the static shading cases that persist for longer duration can occur due to neighboring built structures, etc., are also considered. Out of 11 considered shading cases, the existing OE generates the highest output during four cases, OEP during only two cases and CBM during three cases. In some cases, the existing techniques exhibit poor performance due to their ineffective shade dispersal thus offering reduced output even compared to TCT. Hence, they fail to provide a superior and consistent performance under shading conditions. However, the proposed ACM yields the highest output during all 11 cases, offering a consistently superior performance due to its effective shade dispersal (Fig. 22). The obtained experimental results (shown in Fig. 23) are compared with the simulation results (Table 7 and Fig. 24) and are found to be closer to each other.

6.4 Compatibility and Generalization of the Proposed Technique. In contrast to many static reconfiguration techniques [7–17,19–23,26–28] reported in the literature including CBM, the existing OE, OEP, and the proposed ACM techniques are applicable to all array sizes and can be generalized. To validate the compatibility and effectiveness of ACM for unsymmetrical PV arrays, a 6 × 9 PV array is tested and analyzed under six shading conditions as shown in Fig. 26. The original 6 × 9 matrix and its corresponding

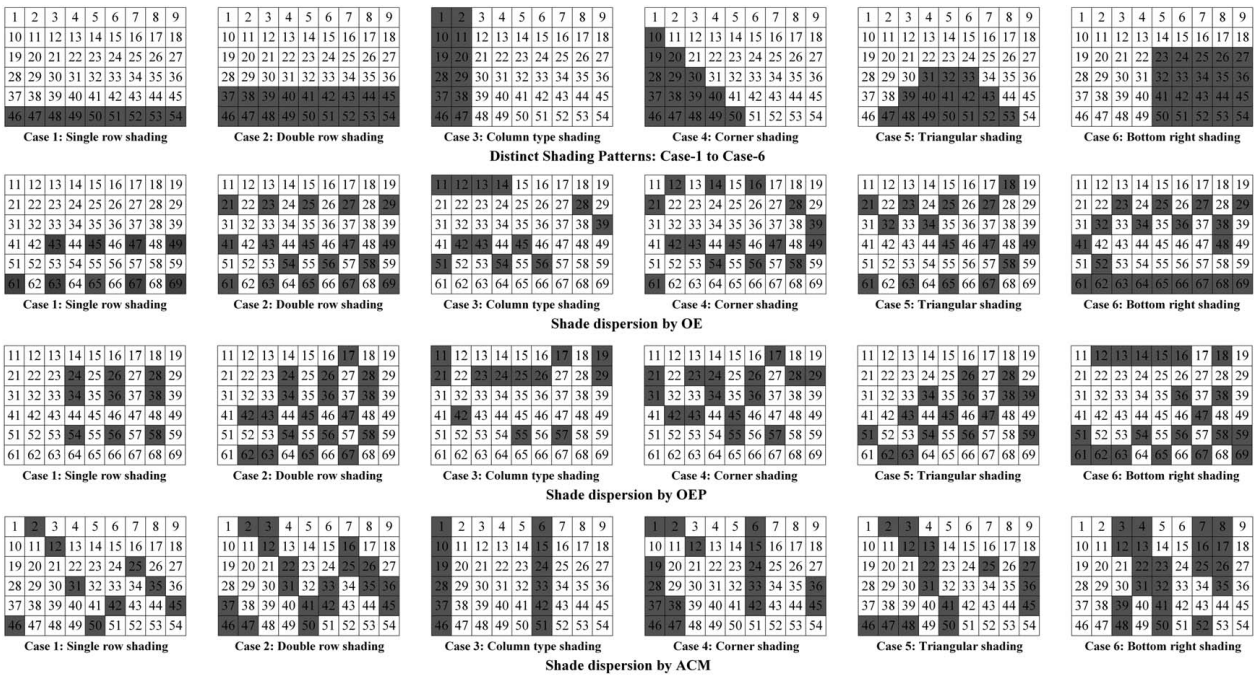

Fig. 26 Distinct shading cases of 6 × 9 array and its corresponding shade dispersion with OE, OEP, and ACM

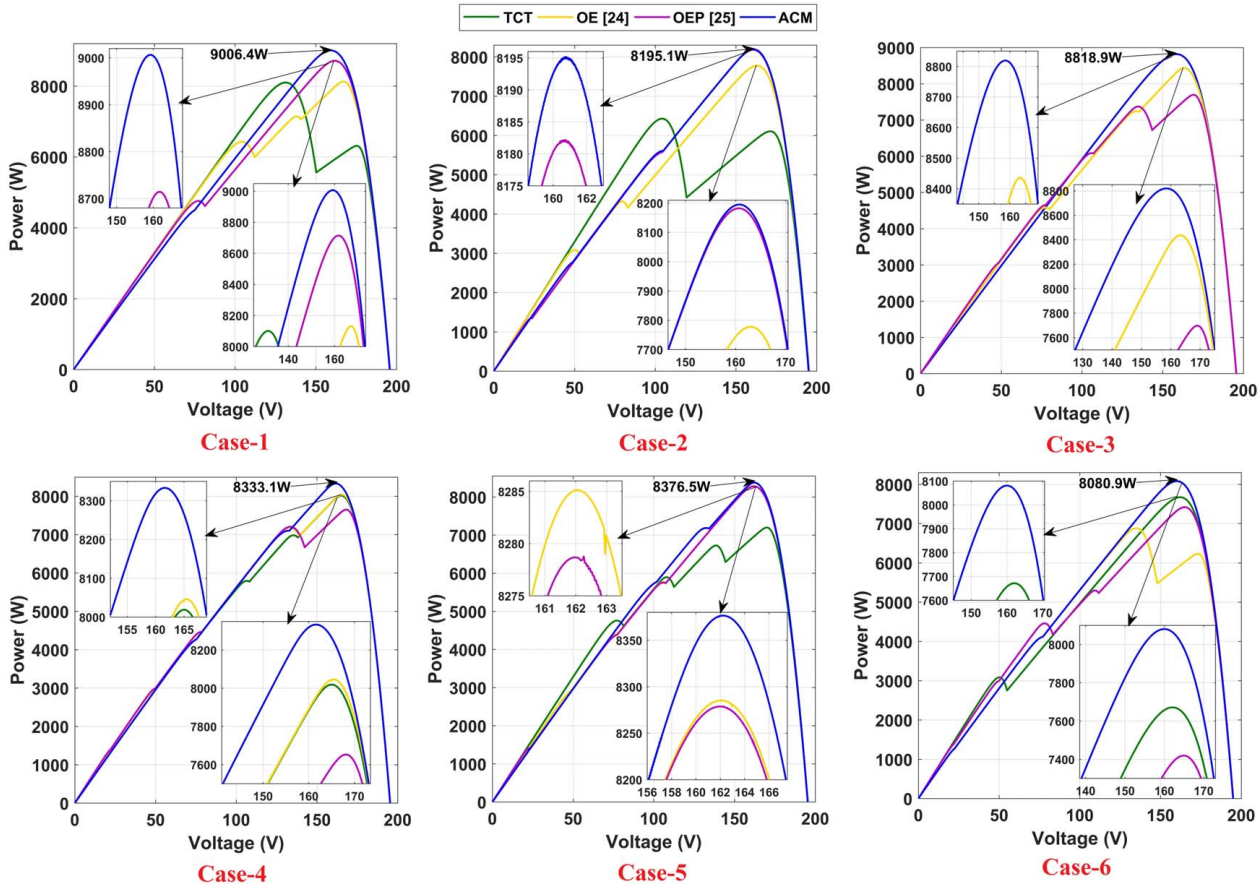

Fig. 27 Power–voltage characteristics of 6 × 9 array under case-1 to case-6 shading (at $T = 25$ °C)

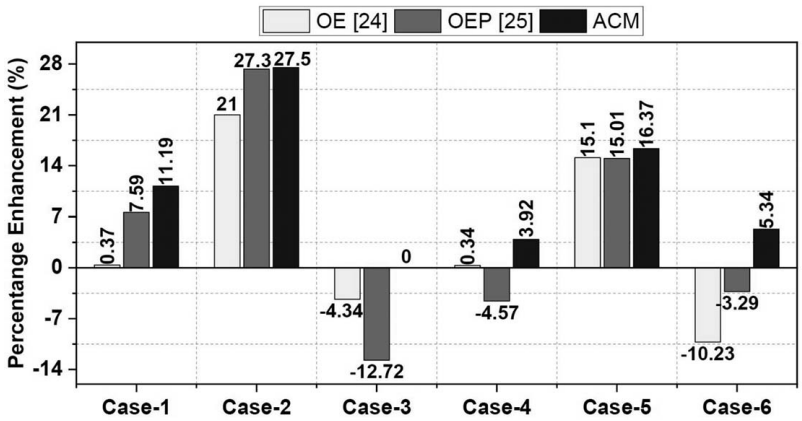

Fig. 28 GMP enhancement of a 6 × 9 array under case-1 to case-6 shading (at $T = 25$ °C)

reconfigured matrix obtained by OE, OEP and the proposed ACM is shown in Fig. 25.

By employing ACM, the shade is effectively dispersed as shown in Fig. 26 and yields enhanced PV characteristics with the highest GMP as shown in Fig. 27. On contrary to existing OE, OEP which offer an inconsistent performance, the ACM yields consistently superior perforamnce which is noted from Table 8 and Fig. 28. Despite being applicable to all array sizes, the existing OE [24], OEP [25] techniques has poor shade dispersion capability, leading to suboptimal solution for shading related issues.

7 Conclusions

In this work, the concept of chaotic map-based approach named Arnold's cat map, a widely utilized tool in image encryption is exercised to reconfigure the PV array for uniform shade dispersal. The compatibility and effectiveness of the proposed ACM is validated for both symmetrical and unsymmetrical PV arrays under various shading cases. The ACM technique substantiated its superior performance over existing SP, TCT, and CBM, OE, OEP configurations with the optimal values of GMP, MM_P, FF, η, Y_A, CF, and

PR under all the shading conditions. Due to their poor shade dispersal ability, the existing configurations exhibit inconsistent performance exhibiting numerous MPPs and reduced output in some shading conditions. On the contrary, the proposed ACM uniformly disperses the shade mitigating the row current mismatch and MPPs yielding maximum output exhibiting consistently superior performance under all shading conditions. Besides, the proposed configuration for a 4 × 4 PV array is validated experimentally in a real-time environment under artificially created static and dynamic shading cases. From the comprehensive analysis, it has been proved that the proposed technique is the best suitable solution for mitigating the shading effects as it reduces the correlation between the adjacent shaded panels in a row by employing the concept of image encryption. This makes the proposed ACM technique unique in solving the partial shading problem.

Conflict of Interest

There are no conflicts of interest.

Nomenclature

A = module dimensions (mm^2)
G = amount of solar irradiation (W/m^2)
I = cell output current (A)
K = Boltzmann constant
T = temperature of the module (°C)
GMP_{PS} = global maximum power at STC (W)
GMP_{STC} = global maximum power under shading (W)
I_d = diode current (A)
I_{mpp} = current at maximum power point (A)
I_o = module reverse saturation current (A)
I_{ph} = photon current (A)
I_{sc} = short circuit current (A)
MM_P = mismatch power loss (W)
N_{pp} = number of parallel-connected PV modules
N_s = number of series-connected cells
N_{ss} = number of series-connected PV modules
R_{se} = series resistance (Ω)
R_{sh} = shunt resistance (Ω)
V_{mp} = voltage at maximum power point (V)
V_{oc} = open circuit voltage (V)
V_{pv} = cell output voltage (V)
V_t = thermal voltage (V)
α = diode ideality factor

Appendix

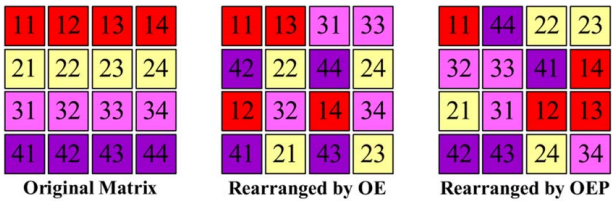

Fig. 29 Original and rearranged 4 × 4 matrix obtained by OE and OEP techniques

Table 9 Specification of PV panel used in experimentation

Parameter	Specification
Maximum power, P_{MPP}	3 W
Open circuit voltage, V_{oc}	10.8 V
Short circuit current, I_{sc}	0.38 A
Maximum power voltage, V_{MPP}	9.01 V
Maximum power current, I_{MPP}	0.34 A

References

[1] Liu, L., and Liu, C., 2013, "A Novel Combined Particle Swarm Optimization and Genetic Algorithm MPPT Control Method for Multiple Photovoltaic Arrays at Partial Shading," ASME J. Energy Resour. Technol., **135**(1), p. 012002.
[2] Pathak, P. K., Yadav, A. K., and Alvi, P. A., 2020, "Advanced Solar MPPT Techniques Under Uniform and Non-Uniform Irradiance: A Comprehensive Review," ASME J. Sol. Energy Eng., **142**(4), p. 040801.
[3] El Iysaouy, L., Lahbabi, M., Baskys, A., and Oumnad, A., 2020, "Performance Analysis of Partially Shaded Photovoltaic Array Using Magic Square View Configuration for Shade Dispersion," ASME J. Sol. Energy Eng., **142**(6), p. 064502.
[4] Ngoc, T. N., Phung, Q. N., Tung, L. N., Sanseverino, E. R., Romano, P., and Viola, F., 2017, "Increasing Efficiency of Photovoltaic Systems Under Non-Homogeneous Solar Irradiation Using Improved Dynamic Programming Methods," Sol. Energy, **150**, pp. 325–334.
[5] Mahmoud, Y., and El-Saadany, E. F., 2017, "Enhanced Reconfiguration Method for Reducing Mismatch Losses in PV Systems," IEEE J. Photovoltaics, **7**(6), pp. 1746–1754.
[6] Ajmal, A. M., Ramachandaramurthy, V. K., Naderipour, A., and Ekanayake, J. B., 2021, "Comparative Analysis of Two-Step GA-Based PV Array Reconfiguration Technique and Other Reconfiguration Techniques," Energy Convers. Manage., **230**, p. 113806.
[7] Rani, B. I., Ilango, G. S., and Nagamani, C., 2013, "Enhanced Power Generation From PV Array Under Partial Shading Conditions by Shade Dispersion Using Su Do Ku Configuration," IEEE Trans. Sustain. Energy, **4**(3), pp. 594–601.
[8] Krishna, S. G., and Moger, T., 2019, "Optimal SuDoKu Reconfiguration Technique for Total-Cross-Tied PV Array to Increase Power Output Under Non-Uniform Irradiance," IEEE Trans. Energy Conv., **34**(4), pp. 1973–1984.
[9] Sai Krishna, G., and Moger, T., 2019, "Improved SuDoKu Reconfiguration Technique for Total-Cross-Tied PV Array to Enhance Maximum Power Under Partial Shading Conditions," Renewable Sustainable Energy Rev., **109**, pp. 333–348.
[10] Tatabhatla, V. M. R., Agarwal, A., and Kanumuri, T., 2019, "Performance Enhancement by Shade Dispersion of Solar Photo-Voltaic Array Under Continuous Dynamic Partial Shading Conditions," J. Cleaner Prod., **213**, pp. 462–479.
[11] Tatabhatla, V. M. R., Agarwal, A., and Kanumuri, T., 2021, "Performance Improvement by Mitigating the Effects of Moving Cloud Conditions," IEEE Trans. Power Electron., **36**(4), pp. 4214–4223.
[12] Horoufiany, M., and Ghandehari, R., 2018, "Optimization of the Sudoku Based Reconfiguration Technique for PV Arrays Power Enhancement Under Mutual Shading Conditions," Sol. Energy, **159**, pp. 1037–1046.
[13] Horoufiany, M., and Ghandhari, R., 2018, "A New Photovoltaic Arrays Fixed Reconfiguration Method for Reducing Effects of One- and Two-Sided Mutual Shading," ASME J. Sol. Energy Eng., **141**(3), p. 031013.
[14] Venkateswari, R., and Rajasekar, N., 2020, "Power Enhancement of PV System Via Physical Array Reconfiguration Based Lo Shu Technique," Energy Conv. Manag., **215**, p. 112885.
[15] Meerimatha, G., and Rao, B. L., 2020, "Novel Reconfiguration Approach to Reduce Line Losses of the Photovoltaic Array Under Various Shading Conditions," Energy, **196**, p. 117120.
[16] Sagar, G., Pathak, D., Gaur, P., and Jain, V., 2020, "A Su Do Ku Puzzle Based Shade Dispersion for Maximum Power Enhancement of Partially Shaded Hybrid Bridge-Link-Total-Cross-Tied PV Array," Sol. Energy, **204**, pp. 161–180.
[17] Reddy, S. S., and Yammani, C., 2020, "A Novel Magic-Square Puzzle Based One-Time PV Reconfiguration Technique to Mitigate Mismatch Power Loss Under Various Partial Shading Conditions," Optik, **222**, p. 165289.
[18] Sai Krishna, G., and Moger, T., 2019, "Reconfiguration Strategies for Reducing Partial Shading Effects in Photovoltaic Arrays: State of the Art," Sol. Energy, **182**, pp. 429–452.
[19] Pillai, D. S., Rajasekar, N., Ram, J. P., and Chinnaiyan, V. K., 2018, "Design and Testing of Two Phase Array Reconfiguration Procedure for Maximizing Power in Solar PV Systems Under Partial Shade Conditions (PSC)," Energy Convers. Manage., **178**, pp. 92–110.
[20] Madhanmohan, V. P., Nandakumar, M., and Saleem, A., 2020, "Enhanced Performance of Partially Shaded Photovoltaic Arrays Using Diagonally Dispersed Total Cross Tied Configuration," Energy Sources Part A, pp. 1–19.
[21] Pillai, D. S., Ram, J. P., Nihanth, M. S. S., and Rajasekar, N., 2018, "A Simple, Sensorless and Fixed Reconfiguration Scheme for Maximum Power Enhancement in PV Systems," Energy Convers. Manage., **172**, pp. 402–417.
[22] Tatabhatla, V. M. R., Agarwal, A., and Kanumuri, T., 2019, "Improved Power Generation by Dispersing the Uniform and Non-Uniform Partial Shades in Solar Photovoltaic Array," Energy Convers. Manage., **197**, p. 111825.
[23] Tatabhatla, V. M. R., Agarwal, A., and Kanumuri, T., 2021, "A Chaos Map Based Reconfiguration of Solar Array to Mitigate the Effects of Partial Shading," IEEE Trans. Energy Conv., pp. 1–1.
[24] Nasiruddin, I., Khatoon, S., Jalil, M. F., and Bansal, R. C., 2019, "Shade Diffusion of Partial Shaded PV Array by Using Odd–Even Structure," Sol. Energy, **181**, pp. 519–529.
[25] Reddy, S. S., and Yammani, C., 2020, "Odd–Even–Prime Pattern for PV Array to Increase Power Output Under Partial Shading Conditions," Energy, **213**, p. 118780.
[26] Anjum, S., Mukherjee, V., and Mehta, G., 2020, "Hyper SuDoKu-Based Solar Photovoltaic Array Reconfiguration for Maximum Power Enhancement Under Partial Shading Conditions," ASME J. Energy Resour. Technol., **144**(3), p. 031302.

[27] Srinivasan, A., Devakirubakaran, S., and Sundaram, B. M., 2020, "Mitigation of Mismatch Losses in Solar PV System—Two-Step Reconfiguration Approach," Sol. Energy, **206**, pp. 640–654.
[28] Anjum, S., Mukherjee, V., and Mehta, G., 2020, "Advanced SuDoKu-Based Reconfiguration Strategies for Maximum Power Extraction From Partially Shaded Solar Photovoltaic Array," ASME J. Sol. Energy Eng., **143**(6), p. 061003.
[29] Nashih, S. K., Fernandes, C. A. F., Torres, J. P. N., Gomes, J., and Costa Branco, P. J., 2016, "Validation of a Simulation Model for Analysis of Shading Effects on Photovoltaic Panels," ASME J. Sol. Energy Eng., **138**(4), p. 044503.
[30] Bingöl, O., and Özkaya, B., 2018, "Analysis and Comparison of Different PV Array Configurations Under Partial Shading Conditions," Sol. Energy, **160**, pp. 336–343.
[31] Shahna, K. U., and Mohamed, A., 2020, "A Novel Image Encryption Scheme Using Both Pixel Level and Bit Level Permutation With Chaotic Map," Appl. Soft Comput., **90**, p. 106162.
[32] Li, C., Tan, K., Feng, B., and Lu, J., 2022, "The Graph Structure of the Generalized Discrete Arnold's Cat Map," IEEE Trans. Comput., **71**(2), pp. 364–377.
[33] Bao, J., and Yang, Q., 2012, "Period of the Discrete Arnold Cat Map and General Cat Map," Nonlinear Dyn., **70**(2), pp. 1365–1375.
[34] Jenisch, S., and Uhl, A., 2014, "Visual Security Evaluation Based on SIFT Object Recognition," AIAI: IFIP International Conference on Artificial Intelligence Applications and Innovations, Rhodes, Greece, September 19–21, 2014; 436, pp. 624–633.